THREE-DIMENSIONAL BIOPRINTING OF TISSUE CONSTRUCTS WITH LIVE CELLS

by

Saime Burçe ÖZLER

Submitted to the Graduate School of Engineering and Natural Sciences

in partial fulfillment of

the requirements for the degree of

Master of Science

Sabancı University

August, 2014

THREE-DIMENSIONAL BIOPRINTING OF TISSUE CONSTRUCTS WITH LIVE CELLS

Approved By:

Assoc. Prof. Bahattin KOÇ (Thesis Advisor)

Prof. Dr. Erhan BUDAK

Asst. Prof. AlpayTaralp

DATE OF APPROVAL: 06.08.2014

To my family,

THREE-DIMENSIONAL BIOPRINTING OF TISSUE CONSTRUCTS WITH LIVE CELLS

Saime Burçe ÖZLER

Industrial Engineering, MSc. Thesis, 2014

Thesis Supervisor: Assoc. Prof. Bahattin KOÇ

Keywords: 3D bioprinting; direct cell printing, scaffold-free tissue engineering; multicellular aggregates; fibroblasts, endothelial and smooth muscle cells; cell viability and fusion

Abstract

Tissue engineering is an emerging multidisciplinary field to regenerate damaged or diseased tissues and organs. Traditional tissue engineering strategies involve seeding cells into porous scaffolds to regenerate tissue or organs. Bioprinting is a relatively new technology where living cells with or without biomaterials are printed layer-by-layer in order to create 3D living structures. In this research work, novel bioprinting methodologies are developed to fabricate 3D artificial biological structures directly from computer models using live multicellular aggregates. Multicellular aggregates made out of at least two cell types from fibroblast, endothelial and smooth muscle cells are prepared and optimized. A semi-continuous bioprinting approach is proposed in order to extrude cylindrical multicellular aggregates through the bioprinter's glass micro-capillaries. The multicellular pellets are first aspirated into a capillary and then compressed to form a continuous cylindrical multicellular bioink. To overcome surface tension-driven droplet formation, the required compression ratio is calculated based on viscosity of cell suspensions. Using the developed biomodeling and path-planning methods, example vascular structures are bioprinted biomimetically from medical images. Based on the developed bioprinting strategies, multicellular aggregates and their support structures are bioprinted to form 3D tissue constructs with predefined shapes. The results show that the bioprinted 3D constructs fuse rapidly and have high cell viability after printing.

ÜÇ-BOYUTLU DOKU YAPILARININ CANLI HÜCRELER KULLANILARAK BİYO-BASIM YÖNTEMİ İLE ÜRETİMİ

Saime Burçe ÖZLER

Endüstri Mühendisliği, Yüksek Lisans Tezi, 2014

Tez Danışmanı: Doç. Dr. Bahattin KOÇ

Anahtar Kelimeler: 3B Biyoyazıcı; İskelesiz doku mühendsiliği; doğrudan hücre basımı; çok-hücreli agregatlar; fibroblast, endotelvedüz kas hücreleri; hücre canlılığı ve füzyon

Özet

Doku mühendisliği hasarlı veya hastalıklı doku ve organların yeniden oluşturulması ile uğraşan ve gelişmekte olan çok disiplinli bir alandır. Geleneksel doku mühendisliği stratejileri, doku veya organların oluşturulmasında hücrelerin gözenekli doku iskelelerine ekilmesini içerir. Biyobasım, canlı hücrelerin 3B canlı yapılar elde etmek amacıyla biyomalzemeler ile veya tek başlarına katman katman basılmalarını sağlayan yeni bir teknolojidir. Bu araştırmada, canlı çok hücreli agregatlar kullanılarak, bilgisayar modelleri ile 3B yapay, biyolojik yapılar elde etmek amacıyla yeni biyobasımmetodolojileri geliştirilmiştir. Fibroblast, endotel ve düz kas hücrelerinden en az ikisini içeren çok hücreli agregatlar hazırlanmış ve optimize edilmiştir. Biyoyazıcının cam mikro kılcal tüplerinden silindirik çok hücreli agregatlar çıkarabilmek için sürekli biyobasım yaklaşımları getirilmiştir. Çok hücreli peletler öncelikle kılcal tüp içine çekilir ve daha sonra boşluksuz, silindirik, çok hücreli bir biyomürekkep elde etmek amacıyla sıkıştırılır. Yüzey gerilimine bağlı damlacık oluşumunu ortadan kaldırmak için, gerekli sıkıştırma oranı hücre süspansiyonu viskozitesine bağlı olarak hesaplanmıştır. Geliştirilen biyomodelleme ve yol planlaması yöntemleri kullanılarak, çeşitli vasküler yapılar tıbbi görselleri birebir taklit edilerek basılmıştır. Önceden tanımlanmış şekillere sahip 3B doku yapıları oluşturmak için, çok hücreli agregatlar ve onların destek yapıları geliştirilen biyobasım yöntemleri ile basılmıştır. Sonuçlar, biyoyazıcı ile basılan yapıların hızlı bir şekilde füzyon olduğunu ve basım sonrası hücre canlılıklarının yüksek olduğunu göstermiştir.

Acknowledgement

First, I would like to sincerely express my gratitude to my advisor, Dr. Bahattin Koc, for his constant motivation, guidance and patience throughout my Master study and helping me with my professional development. I am thoroughly thankful and appreciative of his devotion, direction and encouragement.

I would also like to thank my committee members Dr. Alpay Taralp and Dr. Erhan Budak for their participation, time, and helpful suggestions to improve my thesis. Especially, I am grateful to Dr. Alpay Taralp for his guidance in biomaterials.I would also like to acknowledge Prof. Dr. Mustafa Çulha and his doctoral students Mine Altunbek and Gamze Kuku for their constant support and valuable contributions in the biological part of this thesis.

I would like to thank Sabanci University for supporting me financially through Integral Grant.

It is a pleasure to thank Can Küçükgül who has been my co-worker during last two years. His work ethic and constant friendship made my graduate studies unforgettable. I have been fortunate to be surrounded by friends with whom I could share all my joys and frustrations. I am heartedly thankful to Ecem Ünal, Forough Hafezi, Menekşe Gizem Saygı and Navid Khani.

Alptunç Çomak has been the source of joy, motivation and support in my life. His presence has been meaningful particularly at the difficult times of my Master study. I've been fortunate to encounter him in Sabanci University. I sincerely thank him for his patience, understanding and love.

Finally, I would like to thank my mother Refia Özler, my father Erkan Özler and my lovely sister Burcu Özler for their emotional support during my academic study. I dedicate this thesis to them for being my driving force for all my life.

TABLE OF CONTENTS

LIST OF FIGURES

CHAPTER 1

1. INTRODUCTION

1.1. Tissue Engineering

The loss or failure of an organ or tissue is one of the most devastating, and costly problems in health care. The current treatment methods for organ/tissue loss or failure include transplantation of organs, surgical reconstruction, use of mechanical devices, or supplementation of metabolic products. Tissue engineering is the application of the principles and methods of engineering and the life sciences to the fundamental understanding of structure/function relationships in normal and pathological tissues and the development of biological substitutes to restore, maintain, or improve functions of tissues or organs [1, 2].

Traditionally, tissue engineering strategies are based on the cell seeding into synthetic, biological or composite scaffolds providing a suitable environment for cell attachment, proliferation and differentiation. A scaffold is highly porous complex structure providing an interconnected network that is designed to act as an artificial extracellular matrix (ECM) until the cells form their own ECM. In the late 1990s, the images of the mouse growing a human ear made an overwhelming impression all around the world and attempts have been made on creating tissues or organs in vitro by fabricating cell-seeded scaffolds composed of several bio-compatible materials [3]. In scaffold-based tissue engineering, three steps must be followed including finding a source of precursor cells from the patient, seeding these cells in vitro into the desired places of scaffold and surgically implanting the scaffold into the patient [3].

Bioengineered tissue scaffolds attempt to mimic both the external shape and internal architecture of the replaced tissues. The modeling of scaffolds has a great impact on the growth and proliferation of cells and a spatially and temporally controlled scaffold design could improve cell growth and differentiation. Although many different scaffold manufacturing techniques such as salt-leaching, porogen melting, gas foaming, electrospinning, fiber deposition, molding and freeze-drying have been investigated in the past, these methods cannot control pore size, porosity, pore interconnectivity and external geometries of scaffolds. In recent years, various additive manufacturing methods have been used for biomanufacturing of complex three-dimensional (3D) tissue scaffolds to overcome the limitations of conventional tissue engineering methods [4]. Additive manufacturing techniques allow to fabricate scaffolds layer-by-layer with controlled external and internal geometries based on computer-aided models of targeted tissues[5]. Several researchers have investigated designing functionally gradient porous scaffolds with controllable variational pore size and heterogeneous porous architecture [6, 7].

In scaffold-based tissue engineering, different biomaterials are used for scaffold fabrication such as porous materials composed of biodegradable polymers (polylactic acid, polyglycolic acid, hyaluronic acid and several copolymers), hydroxyapatite or calcium phosphate-based materials and soft materials like collagens, fibrin, and various hydrogels. Although there is a plenty of choice for scaffold materials, those materials should fulfill the requirements to avoid the problems related with scaffold-based tissue engineering. An ideal biomaterial for scaffold fabrication should be nontoxic, nonimmunogenic, capable of maintaining mechanical integrity for tissue growth and differentiation with controlled degradation [3].

After implantation of a scaffold, it should degrade in a controlled manner and the seeded cells should proliferate and migrate into scaffold to replace the scaffold biomaterial. Newly-formed extracellular matrix (ECM) fills the places which were previously occupied by the biomaterial of scaffolds. However, there are some drawbacks to create tissues with biodegradable scaffolds. Mostly, oxygen/nutrient delivery and removal of metabolic waste are insufficient through the micro-channels of a scaffold. Additionally, biodegradation of the scaffold induces inflammation. Even though the biomaterials used may not be directly toxic, they can be metabolized to toxic products [8].

Therefore, several studies are focused on developing infection-resistant biomaterials for scaffold-based tissue engineering, which have also clinical potential. Nonetheless, there are still significant safety problems to be solved.

1.2. Scaffold –free Tissue Engineering

Taking into account all the above mentioned drawbacks, recent tissue engineering studies tends towards ‘scaffold-free’ techniques. In a scaffold-free system, the aim is to obtain a cell-only end product. Even biomaterials are used during fabrication; they are not implanted along with the cells [3].

Most of the scaffold-free approaches use cell sheets or spherical/cylindrical cell aggregates as essential building blocks for implantable 3D constructs. Among the scaffold-free fabrication techniques, cell sheet technology is one of the clinically successful methods for construction of implantable engineered tissues. In this method, cells can be removed from a culture dish as a relatively stable confluent monolayer sheet without destroying cell-cell contacts. This technology has been applied clinically for the repair of skin, cornea, blood vessels, and cardiomyocyte patches to repair partial heart infarcts. In order to build a substantial 3D tissue volume, many sheets need to be culminated in high amount of cells which requires vascularization for cell viability [5].

Bioprinting or direct cell writing is an extension of tissue engineering using additive manufacturing technologies including inkjet-based printing, direct laser printing, and extrusion/deposition based bioprinting or direct cell printing [9]. In comparison to scaffold-based tissue engineering, bioprinting or biofabrication is used to produce complex living and non-living biological products from living cells alone or with biomolecules and biomaterials.

In inkjet-based bioprinting, a bioink made of cells and biomaterials are printed in the form of droplets through cartridges onto a substrate. There are two types of inkjet printing including continuous inkjet printing (CIJ) and drop-on-demand inkjet printing (DOD). In CIJ mode, a jet is obtained by forcing the liquid through an orifice under an external pressure and it breaks up into a stream of droplets. In DOD mode, a pressure pulse is applied into the fluid which generates drops only when needed. Alginate has been used as a constituent of bioink and it was mixed with NIH 3T3 mouse fibroblasts

cell suspension in order to fabricate zigzag cellular tubes with an overhang structure using a platform-assisted 3D inkjet bioprinting system [10].

Laser-based bioprinting methods are suitable for patterning cells by controlling light energy in specific predefined patterns [9]. These laser-based techniques utilize transparent ribbons on which one side is coated with cells that are either adhered to a biological polymer through initial cellular attachment or uniformly suspended in a thin layer of liquid or a hydrogel [9]. A pulsed laser beam is transmitted through the ribbon and is used to push cells from the ribbon to the receiving substrate which is coated with hydrogels. It is also possible to write multiple cell types by selectively transferring different cells to the collector substrate [9]. By using this method, human umbilical vein endothelial cells (HUVEC) are patterned in two- and three-dimensions with micrometer accuracy on Matrigel [11].

The main principle of extrusion-based bioprinting techniques is to force continuous filaments of living cells and biomaterials through a nozzle with a help of a computer to construct a 3D structure [9]. Those systems generally have a fluid-dispensing system and an automated three-axis motion system for extrusion and printing, which provides precise deposition of cells encapsulated in various biocompatible hydrogels. Micro-channels are printed in the form of hallow filaments by using a pressure-assisted layer-based platform equipped with a coaxial needle dispenser unit. Alginate flows between the outer and inner tube of the coaxial nozzle, while calcium chloride as a crosslinker is fed through the inner tube to create the hollow filament. The created micro-channel network does not require any post-processing and shows great potential in perfusing media [12].

Although inkjet bioprinting has been one of the most commonly used method in printing living cells and biomaterials, cell aggregation, sedimentation and cell-damage because of the high shear stresses are common drawbacks of this method. Laser-based cell writing methods are also very versatile and can precisely pattern the cells. However, most of these methods are limited to two-dimensional patterning and it is difficult to fabricate three-dimensional tissue constructs because of process-induced cell injury. The thermal stress and ultraviolet radiation caused by laser printing could also affect the cell viability. There are also several challenges related to extrusion-based bioprinting of cell-laden hydrogels. Hydrogel material used for cell encapsulation could limit cell-cell

interaction and extracellular matrix (ECM) formation. Because of weak mechanical properties of hydrogels, the printed structures have lack of mechanical integrity and it is difficult to form complex 3D structures. Hydrogels used for printing could also cause immunogenic reactions after implantation[9].

1.3. 3D Bioprinter – NovoGen MMX^{TM}, Organovo

The bioprinter used throughout this research is NovoGen MMX^{TM} (Organovo) which is an automated, flexible platform designed to fabricate 3D tissue engineered cell constructs. The 3D bioprinter can print hydrogel biomaterials as well as cylindrical cell aggregates and it fits into a standard biosafety cabinet to provide a sterile operation. The bioprinter has a precision X-Y-Z motion system and two deposition heads as shown in Figure 1.1. The motion system's positional repeatability is approximately ±10 μm, and the positional accuracy between the two deposition heads is maintained with a laser-based calibration system. The deposition heads are equipped with 250/500 μm diameter sized dispensing glass capillaries. Cell capillaries are 75 mm long, while gel capillaries are 85 mm long. The bioprinter has heating and cooling chambers with temperature ranges from room temperature to 95°C and from 4°C to room temperature, respectively. The print stage can be adjusted for standard 100 or 150 mm petri dishes.

Thermoreversible hydrogel is loaded to the bioprinter by immersing the glass capillary fitted with a motorized piston in a vial placed in the heating chamber. The upward movement of the piston aspirates the hydrogel into the capillary. Afterwards, the loaded capillary is immersed in phosphate-buffered saline (PBS) solution at 4°C for a specific time. This time can vary based on the hydrogel gelation properties. The metallic piston is pushed down against the gelled material while the dispense speed and the coordinated movement of the motorized X-Y-Z stages can be controlled via the bioprinter's software. Cell aggregates are also loaded to the bioprinter and extruded in a similar way, which minimizes the shear forces on the cells and sustain cell viability.

While it is possible to control the printer with its own software for simple geometries, novel path planning strategies for both cell and support material must be developed for complex geometries. A custom program can be created by using pre-defined commands with user-specified parameters. The 3D bioprinter can then be controlled directly by the

generated scripts and it can print cell aggregates and support hydrogels layer by layer to form the designed tissue structure.

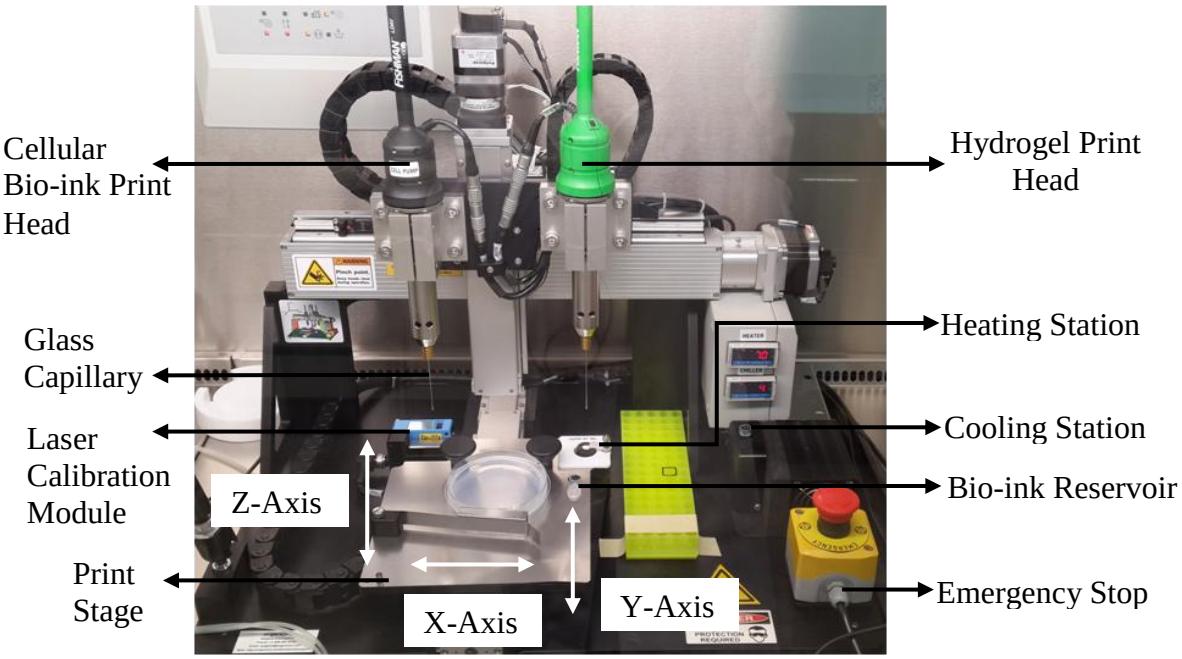

Figure 1.1. 3D Bioprinter, NovoGen MMX^{TM}

The NovoGen MMX^{TM} bioprinting relies on the principle that cell aggregates can successfully be used as building blocks in bioprinting technologies without addition of biomaterials. If multicellular cell aggregates are embedded in appropriately chosen biomaterials they can fuse to form tissue constructs of desired shape based on the concept of tissue liquidity. The liquid-like behavior of cell populations and tissues is explained with differential adhesion hypothesis (DAH) of Steinberg. According to this theory, developing tissues mimic the behavior of highly viscous, incompressible liquids. This liquid-like behavior induces the fusion of two or more adjacent tissue droplets into a single cellular spheroid, and segregation or sorting of various cell types in heterotypic cell mixtures [13].

Traditionally, cylindrical multicellular aggregate preparation includes several incubation steps and manual aspiration of cells in the capillary repetitively. This preparation protocol is involved with human intervention and long incubation periods of cell aggregates slowing down the printing process. In this research, novel bioprinting methods are proposed to create 3D artificial biological structures by semi-continuously depositing cylindrical multicellular aggregates layer-by-layer. Bioink made out of multicellular aggregates, a mixture of at least two cell types, fibroblast, endothelial, and

smooth muscle cells are prepared and optimized for bioprinting. A semi-continuous and computer-controlled bioprinting method is proposed to avoid human intervention and long incubation periods of cell aggregates. For semi-continuous extrusion of cell aggregates and to avoid surface-tension driven droplet formation, aspirated cells are compressed based on the required viscosity of cell suspension. Based on the proposed bioprinting strategies, cylindrical multicellular aggregates and their support structures having respective calculated lengths for each layer are bioprinted, so that non-interrupted closed loops of cylindrical multicellular aggregates and support structures are formed.

This procedure increases the contact of cylindrical multicellular aggregates in adjacent bioprinted layers, facilitates the completely or partly fusion of cells in comparison with that between the cells in spherical aggregates and accelerates the maturation process. More significantly, this procedure reduces the human intervention at forming of cylindrical multicellular aggregates and therefore, increases the reproducibility.

1.4. Organization of Thesis

The presentation of the thesis is organized as follows: a literature review is presented in Chapter 2, semi-continuous cell printing and related implementation and analyses are explained in Chapter 3, modeling of direct cell writing is presented in Chapter 4. Furthermore, 3D bioprinting of biomimetic aortic tissue constructs is presented in Chapter 5. Finally, conclusions are drawn in Chapter 6.

CHAPTER 2

2. LITERATURE REVIEW

Although there is an increase in willing donors, the chronic lack of replacement organs is a current problem all around the world. Alone in the United States, it is estimated that about 6000 people are waiting for kidney transplants, 3000 for heart transplants and 17000 for liver transplants [14]. In Turkey, it is reported that approximately 25 000 people are in waiting list for kidney transplantation, 2000 for liver transplantation and 500 for heart transplantation [15]. The situation is even more dramatic for cardiovascular diseases. According to the American Heart Association, in 2008, an average of one death occurred every 39 seconds due to cardiovascular diseases which accounts to more than 2200 deaths each day in the United States. Not only in the United States, cardiovascular diseases are the primary reasons of deaths and they rank among the top ten leading causes of morbidity and mortality [16]. According to the report of the Turkish Society of Cardiology, in 2005, around 2,8 million people suffered from cardiovascular diseases. Cardiovascular health diseases are mostly treated with synthetic grafts, which are especially convenient for the treatment of large arteries, whereas their use in small-diameter blood vessels such as coronary or below the knee arterial is infeasible due to their low patency [17]. Moreover, synthetic grafts may trigger chronic inflammation leading to a late graft failure, bacterial colonization and graft infection directly related to mortality and amputation rates. In order to eliminate the adverse effects of synthetic grafts, attempts have been made to produce a tissue engineered vascular grafts composed of biological materials and autologous cells. The living graft has an inherent healing potential and the body can remodel its biological matrix according to requirements of the environment. Most significantly, foreign body reaction and graft infection can be reduced or eliminated resulting in complete graft integration and increased overall patency rates.

Recently, there have been a few studies focusing on vascular and valve tissue engineering using bioprinting techniques. Valve scaffold tissue engineering has the potential for fabricating aortic valve hydrogel scaffolds that can grow, remodel and integrate with the patient. In order to mimic complex 3D anatomy and heterogeneity of aortic valve, root wall and tri-leaflets were 3D printed with poly-ethylene-glycol-diacrylate (PEG-DA) hydrogels. Porcine aortic valve interstitial cells (PAVIC) seeded scaffolds maintained near 100% viability over 21 days [18]. Another study demonstrated that encapsulated aortic root sinus smooth muscle cells (SMC) and aortic valve leaflet interstitial cells (VIC) were viable within the bioprinted alginate/gelatin aortic valve hydrogel conduits [19].

Latest 3D tissue engineering approaches also tend towards bioprinting of cell-laden hydrogels. Human mesenchymal stem cells were encapsulated into agarose hydrogels and cell-laden hydrogel was 3D printed submerged in a hydrophobic high-density fluorocarbon, which mechanically supports the construct and afterwards can be easily removed [20]. This method allows high stability to the printed structures, high cell viability, cell proliferation and production of extracellular matrix (ECM) [20]. Additionally, cell-laden microengineered hydrogel constructs with an embedded network of vascular-like microchannels were sequentially assembled in a biphasic reactor in order to achieve 3D tubular constructs. The assemble of endothelial cells and smooth muscle cells encapsulated in hydrogels resulted in a blood vessel-like structure demonstrating this approach as a simple and rapid biofabrication method [21]. Furthermore, another 3D micromolding technique was proposed in order to bioprint microchannel networks for controlled vascularization within hydrogel based engineered tissue constructs. After bioprinting of agarose fibers with well-defined and controlled architecture, methacrylated gelatin (GelMA), star poly(ethylene glycol-co-lactide) acrylate (SPELA), poly(ethylene glycol) dimethacrylate (PEGDMA) and poly(ethylene glycol) diacrylate (PEGDA) hydrogels were casted over the bioprinted templates respectively and subsequently photopolymerized. After gelation, agarose fibers can be easily removed from hydrogels without any requirement for template dissolution. Furthermore, microchannels fabricated in cell-laden GelMA exhibit improved mass transport and consequently high viability and differentiation of osteogenic cells [22]. Although there are few studies relevant to the vascular tissue engineering, the poor mechanical strength of the materials compared to native vessels has limited the

construction of an entirely biomimetic blood vessel. Therefore, the first implementations of scaffold-based vascular grafts were examined under low pressure [23]. In addition, chronic inflammation, thrombosis and rejection after *in-vivo* implantation could be unpredictable side effects due to the degradation of the materials and the cell-material interactions. Particularly, fragility of cell to cell interaction and the assembly and alignment of extracellular matrix (ECM) play a crucial role in vascular tissue-engineering [16]. Because of these, recent vascular tissue engineering studies focus on scaffold-free techniques.

In the literature, there have been few research focusing on scaffold-free tissue engineering of small-diameter, multi-layered, tubular vascular and nerve grafts [24]. Different 3D bioprinting systems have been proposed to fabricate vascular structures. A platform-assisted 3D inkjet bioprinting system was utilized in order to fabricate NIH 3T3 mouse fibroblast-based tubes with an overhang structure having a post-printing cell viability above 82% [10]. Furthermore, the direct anastomosis of the tissue-engineered constructs with a functional vasculature to the host vasculature *in vivo* is provided by self-assembly approaches. The autonomous organization of components from an initial state into a final pattern or structure without external intervention is called self-assembly. In the field of tissue engineering, self-assembly occurs in an *in vivo* like, fully controllable cell environment (bioreactor) by the differentiation of cells at the right time, in the right place and into the right phenotype and eventually the assembly of them to form functional tissues. Based on this approach, a perfusion reactor is used for the maturation of a bioprinted macrovascular network in order to obtain the required mechanical properties. Microvascular units consisting of cylindrical or spherical multicellular aggregates were fabricated by the parenchymal and endothelial cells[25]. Afterwards, microvascular units were located in the macrovascular network for the perfusion supporting self-assembly and the connection to the existing network. Multicellular spherical and cylindrical aggregates have been constructed by using 3D printing methods, which enable to achieve flexibility in tube diameter and wall thickness and to form branched tubular structures. However, the printed cell aggregates should be perfectly supported by hydrogels for 3D printing. In another study, human embryonic stem cell spheroid aggregates consisting controllable and repeatable sizes were fabricated with a valve-based cell printer. According to that work, the printed stem cells have high viability after printing and are able to differentiate into any of the three

germ layers [26]. Nevertheless, the formation of large amounts of spherical aggregates requires a lot of time and the fusion process of the spheroids is completed in 5-7 days. Conversely, it is possible to fabricate more controlled structure in a short time using cylindrical cell aggregates (bioink). Moreover, the fusion of cylindrical bioinks takes 2-4 days [23]. In spite of that, 3D printing of complex tissue constructs with cylindrical bioinks faces considerable challenges. These approaches mostly require laborious bioink preparation and rely on one's own skills and therefore cannot be fully automated.

In 1986, Weinberg and Bell produced a tissue engineered blood vessel from a collagen gel model, in which bovine endothelial cells, smooth muscle cells and fibroblasts were embedded for the first time. However, this model did not have the required mechanical strength necessary to sustain normal blood pressure. One of the impressive examples of self-assembly methods is the sheet-based tissue engineering technology which is mainly used for the production of tissue engineered blood vessel (TEBV). L'Heureux and his group produced a tissue engineered blood vessel based on cultured human cells and it contained all three histological layers such as the endothelium, the media and the adventitia. In this self-assembly approach, smooth-muscle cells and fibroblasts were cultured in medium containing serum and ascorbic acid and produced their own extracellular matrix (ECM). The smooth-muscle cell sheet was placed around a tubular mandrel (polytetrafluoroethylene) to produce the media of the vessel. A similar fibroblast cell sheet was wrapped around the media to provide the adventitia after eight weeks of maturation. Finally, the tubular support was removed and endothelial cells were seeded in the lumen to form the endothelium. As projected, the culture period and maturation period directly affects the resulting thickness and the burst strength of adventitia respectively. The tissue engineered blood vessel has burst strength of over 2500 mm Hg which is significantly higher than that of human saphenous veins (1680±307 mm Hg). The transplantation of this blood vessel into dogs demonstrated good handling, suturability by the use of conventional surgical techniques. Since Weinberg and Bell's landmark report, the fundamental challenge in cardiovascular tissue engineering field has been to produce a vessel with requisite mechanical strength without using permanent synthetic scaffolds. Therefore, sheet-based tissue engineering has been used to produce tissue engineered blood vessel (TEBV) suitable for autologous small diameter arterial revascularization in adult patients. Fibroblasts were cultured in conditions promoting extracellular matrix (ECM) deposition to produce a cohesive

sheet that can be detached from the culture flask. This approach also eliminates the use of smooth-muscle cells, whose early senescence is related with decreased burst pressures in human models. The decellularized internal membrane (IM) and living adventitia were assembled by wrapping fibroblast sheets around a temporary Teflon coated stainless steel support tube. After weeks-long maturation and dehydration to form an acellular substrate, the steel tube was removed and endothelial cells were seeded in the lumen of living TEBV. The produced TEBV (internal diameter, ID=4.2 mm) were xenografted in a dog model for short-term evaluation demonstrating positive handling characteristics and suturability. For longer-term *in vivo* evaluation, single layer (without IM) vessels and two-layer TEBV's (ID=1.5 mm) were implanted in nude rats as abdominal interpositional grafts. In single layer vessels, overall patency was 85% up to 225 days. Two-layer vessels demonstrated impressive graft incorporation into the surrounding tissue, no blood infiltration in the wall and no mechanical failures between 90 and 225 days. In order to evaluate the TEBV in a more representative biomechanical environment, human TEBVs (ID=4.2 mm) were implanted as interpositional arterial grafts in immunosuppressed cynomolgus primates. All vessels were patent with smooth lumens, intact anastomoses and no sign of aneurysm formation up to eight weeks. Ultimately, this is an effective approach to produce a completely biological and clinically applicable TEBV in spite of its relatively long production time (≈28 weeks) which clearly prevents its urgent clinical use [27]. Okano and colleagues have developed a method for cell sheet engineering by first coating culture dishes with a temperature-responsive polymer, poly (N-isopropylacrylamide) (PIPAAm). The surface is relatively hydrophobic at 37°C allowing cells to attach and proliferate, while cooling below 32°C (typically 20°C for 30 minutes) makes the surface hydrophilic and causes the cells to detach without the use of enzyme digestion reagent. When grafted PIPAAm layer thickness is between 15 and 20 nm, temperature-dependent cell adhesion and detachment can be observed. Once the cells spread and adhere confluently on the surface, they can be spontaneously detached as a contiguous cell sheet by reducing the temperature. This process does not disrupt the cell-cell junctions because no enzymes like trypsin or chelator such as ethylenediaminetetraacetic acid (EDTA) are required. Additionally, basal surface extracellular matrix (ECM) proteins such as fibronectin are preserved after detachment which enables easily attachment of cell sheets to host tissues and even wound sites with minimal cell loss. In order to obtain tissue constructs with characteristic physiological cellular functions in vitro, heterotypic cell-cell interactions

are inevitable. It is possible to modify the above-mentioned technique in order to develop patterned cell sheets using two or more kinds of cell source. Domains on petri dishes were grafted by using area-selective electron beam polymerization of PIPAAm. After cells were cultured on the patterned grafted surfaces at 37°C, the temperature was decreased to 20°C. Cells on the PIPAAm surface are detached where other cell types were seeded subsequently by increasing the temperature to 37°C. Therefore, two cell types can be co-cultured in desired places which improve cellular functions [8, 28]. Apart from its wide applications, cell sheet technology is a potential and promising approach for the treatment of cardiac diseases. Three-dimensional myocardial tubes were fabricated and transplanted by wrapping cardiomyocyte sheets sequentially around a resected thoracic aorta. Four weeks after aortic replacement, the myocardial tubes were integrated with the host tissues showing spontaneous and synchronized pulsation [28].Tissue-engineered blood vessels have been mainly created by using endothelial cells, smooth muscle cells and biomaterials. However, both endothelial cells (ECs) and smooth muscle cells (SMCs) are difficult to be expanded and proliferation capacity and collagen production of SMCs from elderly persons are reduced after expansion. On the other hand, mesenchymal stem cells (MSCs) can differentiate into multiple cell lines including ECs and SMCs. In order to construct TEBVs suitable for arterial revascularization, rabbit MSCs were cultured in the presence of ascorbic acid to form a cell sheet. The sheets were rolled around a mandrel resulting in a tubular-shape graft with a diameter of about 2 mm and with a thickness of about 0.5 mm according to the hematoxylin and eosin staining. After four weeks implantation of TEBVs into common carotid artery defects of rabbits, TEBVs endothelialized and remodeled themselves in vivo in a similar manner to native artery. These results demonstrate that a completely biological TEBV can be fabricated with autologous MSC sheets without using SMCs, ECs and biomaterials [29]. Although cell sheet-based tissue engineering approaches has been clinically successful, months-long production and creating only simple tubular conduits are the main drawbacks of these methods [30].

Apart from bioprinting and sheet-based tissue engineering, a new method is presented to rapidly self-assemble cells into 3D tissue rings without the use of additional equipment. This method enables fabrication of engineered tissue constructs entirely from cells by seeding cells into custom made annular agarose wells with 2, 4 or 6 mm inside diameters. Different cell types including rat aortic smooth muscle cells and human

smooth muscle cells are used with varying seeding conditions and culture length to form tissue rings. The strength and modulus of tissue rings increased with ring size and decreased with culture duration. Rat smooth muscle cell rings with an inner diameter of 2 mm are cohesive enough for handling after 8 days incubation and they yield at 169 kPa ultimate tensile strength. Furthermore, it is also possible to fabricate tissue tubes by transferring the rings onto silicone tubes, sliding them into contact with one another and incubating them for an additional 7 days. Although these rings are not as strong as ring segments of native blood vessels or TEBV fabricated from cell sheets for 2-3 months, the presented method allows developing strong 3D tissue constructs from aggregated cells within an experimentally useful time frame (1-2 weeks) [31, 32]. Likewise created smooth muscle cell tissue rings and rings fabricated from cells seeded in fibrin or collagen gels are compared based on their relative strength and utility for tissue engineering. All tissue rings were cultured for 7 days in supplemented growth medium which includes ε-amino caproic acid, ascorbic acid, and insulin-transferrin-selenium. Ultimate tensile strength and stiffness values of tissue rings were two-fold higher than fibrin gel and collagen gel rings. Tissue rings cultured in supplemented growth medium exhibit a three-fold increase in tensile strength and stiffness in comparison to the tissue rings cultured in standard growth medium [33].

CHAPTER 3

3. SEMI-CONTINUOUS CELL PRINTING

Three-dimensional bioprinting can be defined as extrusion or deposition of live cells alone or with active biomolecules or biomaterials to create tissue constructs [9]. In the literature, spherical or cylindrical cell aggregates are used as bioink for bioprinting processes [14, 23-25, 34, 35]. However, preparing bioink requires time-consuming manual operation and makes totally automated and computer-controlled 3D bioprinting impossible in earlier studies.

In this chapter, semi-continuous direct multicellular aggregate printing is proposed. Bioinks composed of different combinations of mouse aortic smooth muscle cells (MOVAS), NIH 3T3 mouse fibroblast cells, human umbilical vein endothelial cells (HUVEC), and human dermal fibroblast (HDF) cells are used for semi-continuous bioprinting. Computer-aided semi-continuous and, interconnected tool-path planning methodologies have been developed for a three-dimensional multicellular bioink printing process. The 3D bioprinter is used for precise deposition of multicellular aggregates according to computer-generated paths. Several example regular and free-form geometries are printed using the developed algorithms. The printed 3D multicellular structures are examined for their mechanical strength, shape deformation with time, cell viability and cell fusion.

3.1. Materials and Methods

3.1.1. 3D bioprinter and hydrogel preparation

Cells and support biomaterials are 3D printed using Novogen MMX Bioprinter (Figure 1.1). A biocompatible, bio-inert, thermo-reversible hydrogel, NovoGel (Organovo) was used as the support material. NovoGel 2% (w/v) was prepared with phosphate buffered saline (PBS: Hyclone 1X by Thermo Scientific) with Ca^{2+} and Mg^{2+} salts solution by autoclaving it following the standard liquid sterilization procedures. NovoGel was loaded to the bioprinter by immersing the glass capillary fitted with a motorized piston in a vial placed in the heating chamber with 70°C. The upward movement of the piston aspirates the hydrogel into the capillary. Afterwards, the loaded capillary was immersed in PBS at 4°C for 10 seconds.

3D bioprinting requires a uniformly flat surface. To create a flat surface, 2 % Agarose solution was first prepared with PBS. After a sterilization process, 20 mL agarose solution was transferred into a 100 mm petri dish bottom covering the entire dish bottom surface. A homemade Teflon mold which fits into the petri dish was sterilized and used for providing a flat surface. The mold was carefully put down onto the agarose inside the petri dish. The mold was then carefully taken away from the petri dish after the agarose solution became completely solid gel. Before the use of the base plate (Figure 3.1) for bioprinting, it was washed with PBS [36]. During the materials preparation, adequate sterilization steps are followed to avoid any contamination.

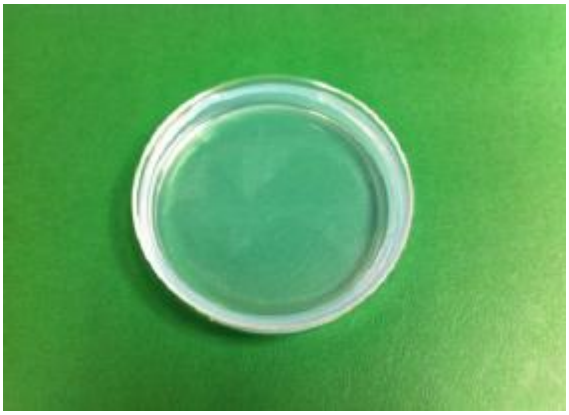

Figure 3.1. Base plate for bioprinting

3.1.2. Cell Culture and preparation of the multicellular bioink

The culture conditions, culture medium and its additives are cell-specific and effective for cell quality. MOVAS (ATCC), NIH 3T3 mouse fibroblast cells (ATCC), HUVEC (ATCC) and HDF (generously provided by Yeditepe University, Turkey) cells were cultured at 37°C in 5% CO_2 using Dulbecco's Modified Eagle's Medium (DMEM, Sigma, Germany) supplemented with 10% fetal bovine serum (FBS, Sigma, Germany), 1% Penicillin-Streptomycin (Sigma, Germany).

The cells were cultured in tissue culture flasks. Following the removal of the culture medium from the culture flasks, the cells were washed with PBS and detached by using cells scrapers. Following the detachment step, the cells were centrifuged at 1100 RPM for 5 minutes, then the supernatant was discarded thus a cell pellet is obtained. After removing the supernatant, the cell pellet was resuspended in a 1 mL medium and transferred into 1.5 mL Eppendorf tubes and centrifuged again at 1000 g (≈3000 RPM) for 5 minutes to form a dense cell pellet.

In the case of HDF cells, once the cell pellet was obtained, it was resuspended in 1 mL of culture medium and transferred into T25 tissue culture flasks (TPP, Germany) containing 6 mL culture medium. T25 tissue flasks were incubated at 37°C and 5% CO_2 on an orbital shaker (using IKA, KS 130 basic, Germany) and shaken at 160 rpm for 60 minutes. Then, the same procedure is followed in order to obtain a dense pellet. This shaking-period is important in order to allow the cells to aggregate and initiate cell-cell adhesion.

For the preparation of multicellular aggregates, MOVAS, HUVEC and NIH 3T3 mouse fibroblast cell suspensions were mixed and densities adjusted to obtain a mixture of MOVAS, HUVEC, NIH 3T3 in a 70:25:5 ratio. On the other hand, HUVEC and HDF cell suspensions were mixed to arrive at a 75% HUVEC / 25% HDF mixture. After discarding the supernatant, the cell pellets in the Eppendorf tubes were non-formed multicellular aggregates to be aspired into capillaries for formation of cylindrical multicellular aggregates (bio-ink) for semi-continuous bioprinting according to the developed algorithms.

The bioprinted constructs were incubated for 1-10 days so that the printed bio-inks fuse together to form an artificial biological tissue network. During the maturation period,

the above mentioned growth medium is supplemented with 0.05 mg/mL L-ascorbic acid (Sigma, A4544), 0.01 mg/mL insulin (Sigma, I9278), 0.01 mg/mL transferrin (Sigma, T8158) and 10 ng/mL sodium selenite (Sigma, S5261). All the media were changed three times weekly.

3.1.3. Semi-Continuous path planning

As mentioned above, semi-continuous bioprinting enables to design and 3D print extruded multicellular aggregates corresponding to any size and shape of a targeted tissue. Therefore, zig-zag and spiral pattern tool-path methodologies are developed to print different shaped structures with multiple layers. Regular circular, rectangular and cylindrical shapes as well as a free-form shape structure are bioprinted to demonstrate that the proposed methodology can print the predefined cellular structures semi-continuously. A CAD software package, Rhino3D using Rhinoscript language, was used for developing semi-continuous and connected bioprinting path plans. The developed path plans for various shapes are rectangular, zig-zag patterned circular, spiral patterned circular, random-shaped and stripe shaped structures which are shown in Figure 3.2-Figure 3.5.The path plans of cellular aggregates are developed so that the cylindrical cellular aggregates are bioprinted adjacently which supports the maturation period. In order to observe the migration and fusion process of the cells, the path plans of cellular aggregates in zig-zag patterned circular structure are generated with a small gap between them (Figure 3.5).

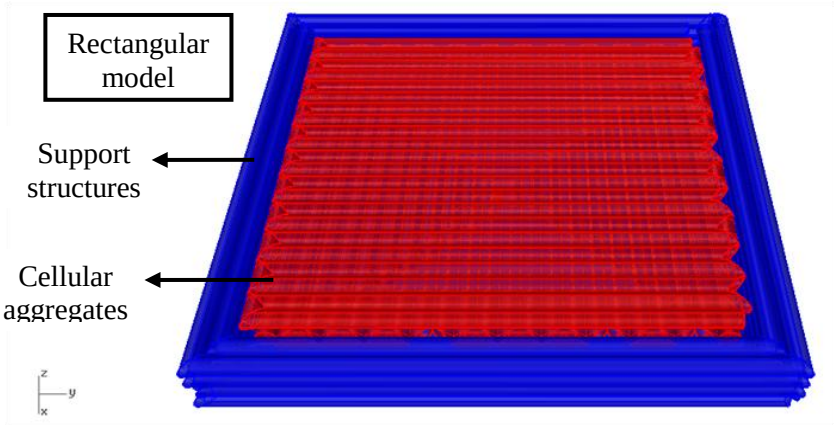

Figure 3.2. Rectangular model

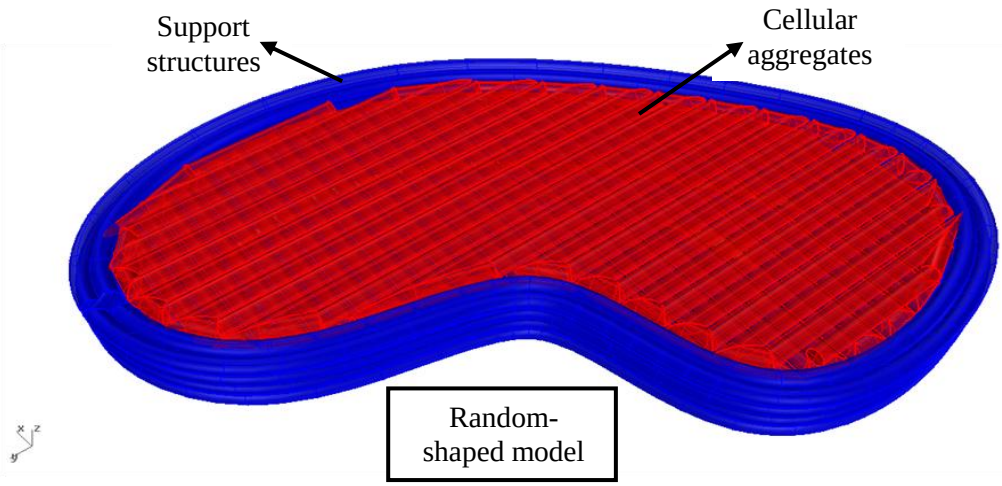

Figure 3.3. Random-shaped model

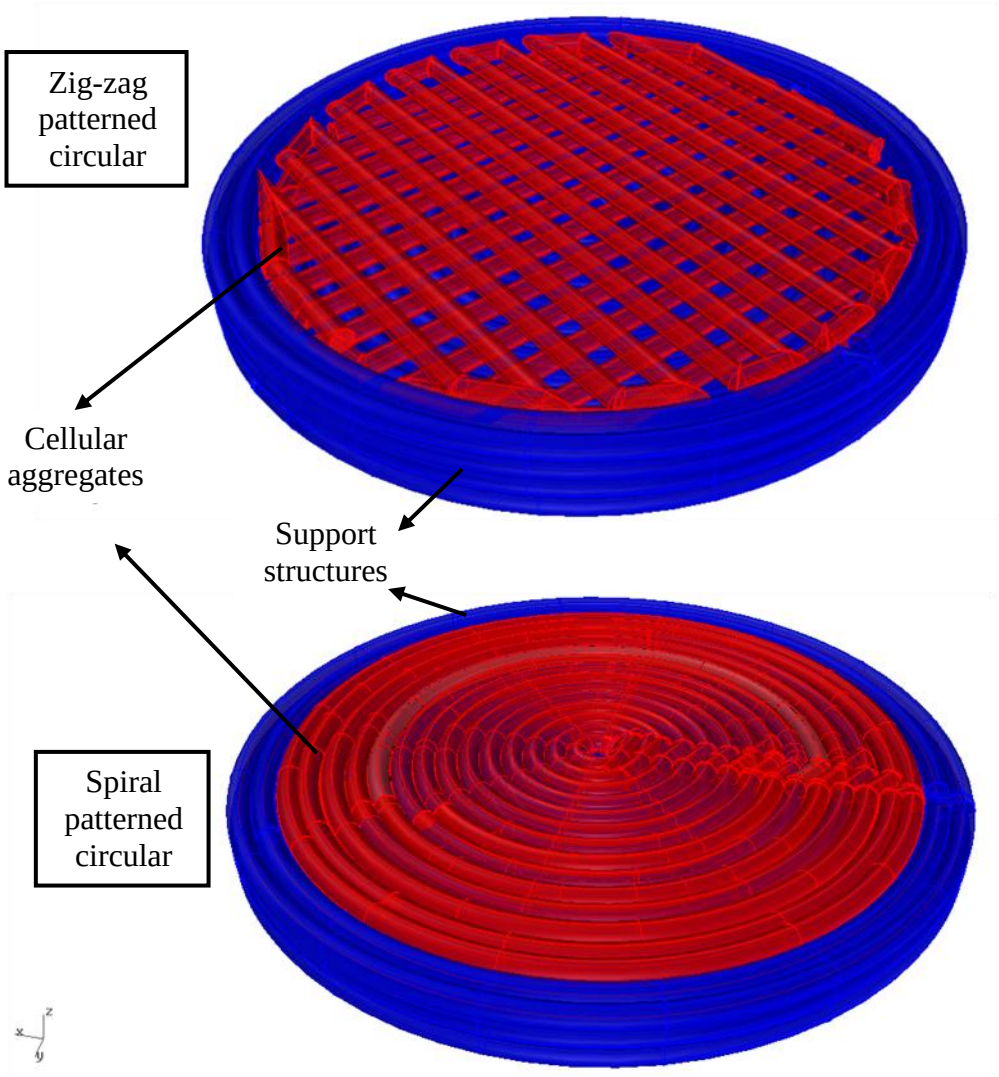

Figure 3.4. Circular models

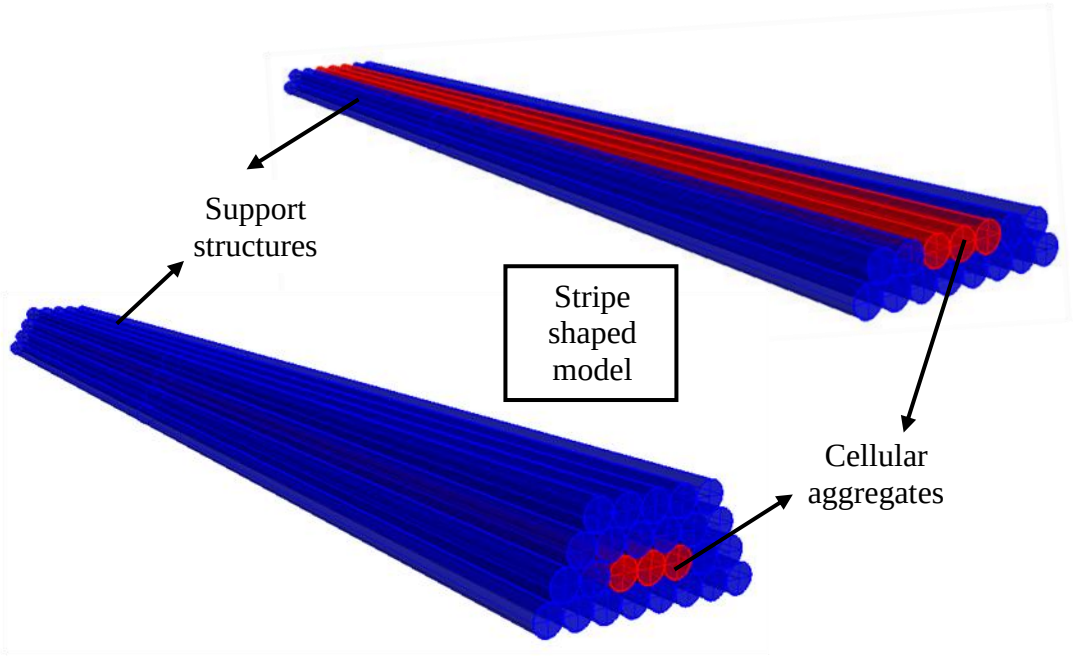

Figure 3.5. Stripe-shaped model

3.1.4. Implementation and Mechanical testing of printed structures

The developed models are used to 3D bioprint cylindrical multicellular aggregates composed of MOVAS, HUVEC and NIH 3T3 cell mixture. HUVEC and HDF cell aggregate mixture was only 3D printed in stripe form because low proliferation rate and long culture period of HDF cell line limits the size of the printed structures. Except the stripe shaped structures, all other models have 2 layers of multicellular aggregates covered with 2 support structure layers.

The printed constructs were incubated 1-10 days to allow them to mature. At specific time points (4-7-10 days) of the maturation period, they were subjected to a mechanical test. Here, the mentioned mechanical test is composed of removal of hydrogel support structures *via* manual pulling and achievement of a cell structure without any integrity loss.

3.1.5. Deformation of the printed structures

After the printing process, the structures were covered with the above mentioned cell culture medium and incubated. During the incubation period, the printed structures were observed in order to investigate their possible shape deformations. The pictures of the printed constructs were taken each day till the end of the specified maturation period. The length or the area of the printed constructs were measured by ImageJ software [37] and their deformation percentages were calculated and compared to the post-printing (i.e. day 0) sizes.

3.1.6. Cell viability and fusion

The cell viability and fusion of the printed cell aggregates are examined using the stripe-shaped printed structure which is shown in Figure 3.6. Before the staining procedure of the printed cell aggregates for viability and fusion evaluation, the support structures are removed manually in order to avoid the possible hydrogel staining which can hamper a good fluorescent illumination. After the removal of the support structure, all the cells of the printed structure are stained for cell viability and fusion examination, respectively.

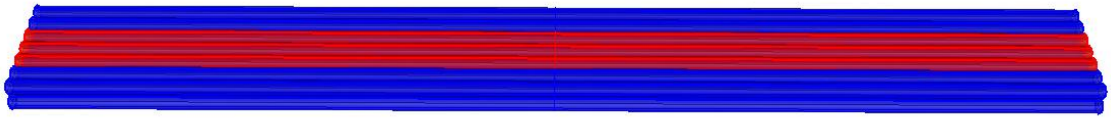

Figure 3.6. Top-view of the stripe-shaped model

The cell viability of post-printed cell aggregates was assessed immediately after printing. The printed cell structures were washed with PBS, resuspended in 2 mL trypsin-EDTA (Sigma) solution and incubated for 10 minutes. Then, 3 mL of DMEM complete cell culture medium was added and resuspended. After 50 µl of cell-medium suspension and 10 µl of 0.5% trypan blue stain (Sigma-Aldrich) were mixed, the cells were viewed and evaluated using an optical microscope. The transparent cells were considered live while the blue cells were considered dead since viable cells with intact cellular membrane excluded the blue dye [10]. The number of live/dead cells was counted twice to get an average cell viability value.

The cell viability after 3 and 7 days was determined using a Live/Dead assay Kit. The cells were stained with calceinacetoxymethylester (calcein AM) and propidium iodide (PI, Invitrogen), at a concentration of 1.5 μg/mL each. Green-fluorescent calcein-AM indicates intracellular esterase activity in live cells, while propidium iodide (PI) is a popular red-fluorescent nuclear and chromosome counterstain, which is not permanent to live cells and therefore commonly used to detect the dead cells in a population. After the cell structure was trypsinized, DMEM complete cell culture medium was added and the cell-medium suspension was centrifuged. Then, the supernatant was removed; the cells were washed with PBS and centrifuged. First, the cells were stained with calcein AM by keeping them at 4°C for 15 minutes. Then, the cells were washed with PBS and stained with PI by keeping them at room temperature for 15 minutes. Finally, the staining medium was aspirated, formaldehyde was added on the cells and they were kept at 4°C for 30 minutes. Before fluorescent illumination, the formaldehyde was removed and PBS was added to wash off any residual formaldehyde on the cells. The cells were imaged using an Olympus IX70 fluorescent microscope. The number of live and dead cells was counted using ImageJ software. Once the green- and the red-stained cells were counted, the percentage of viable cells was calculated based on the number of live cells divided by the total cell number.

In order to visualize the fusion of cylindrical multicellular aggregates, cells were stained with green or red membrane-intercalating dyes (SP-DilC18 and SP-DiOC18, Molecular Probes) before detaching them from the cell culture flasks. Each dye with a concentration of 1.5 μg/mL was separately added into serum free DMEM complete cell culture medium. The cells were washed with PBS and incubated for 30 minutes with the dyed medium to make cylindrical multicellular aggregates of different fluorescent colors. After staining, the cells were prepared for printing as explained above.

3.2. Results and Discussion

3.2.1. Implementation of the developed models

Based on the developed models, the multicellular bioink composed of MOVAS, HUVEC and NIH 3T3 cells was 3D bioprinted having rectangular, zig-zag patterned circular, spiral patterned circular, random-shaped and stripe shaped structures. Figure 3.7-Figure 3.9 show the printing process of support structures and cylindrical multicellular bioink.

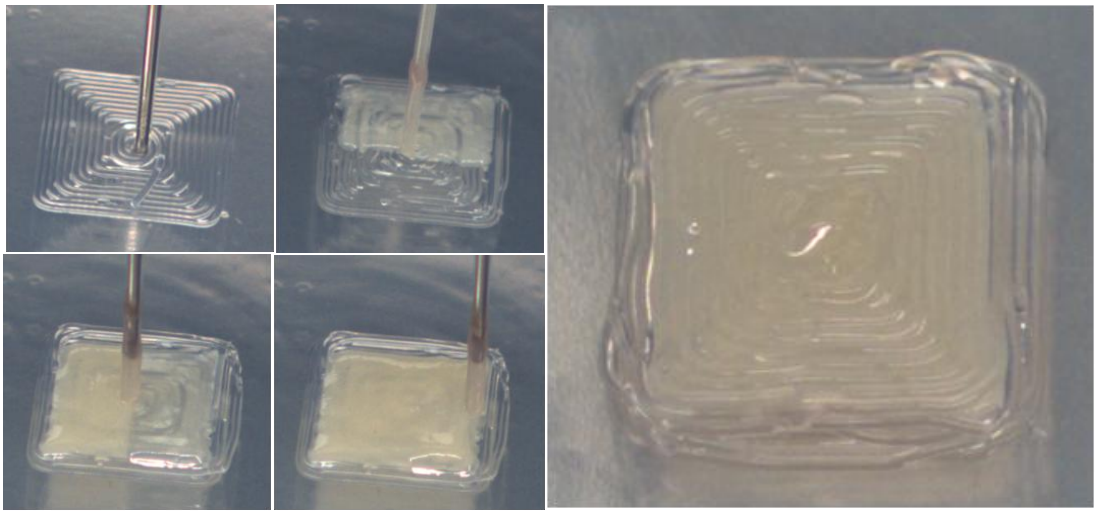

Figure 3.7. Rectangular shaped printed structure (zig-zag path)

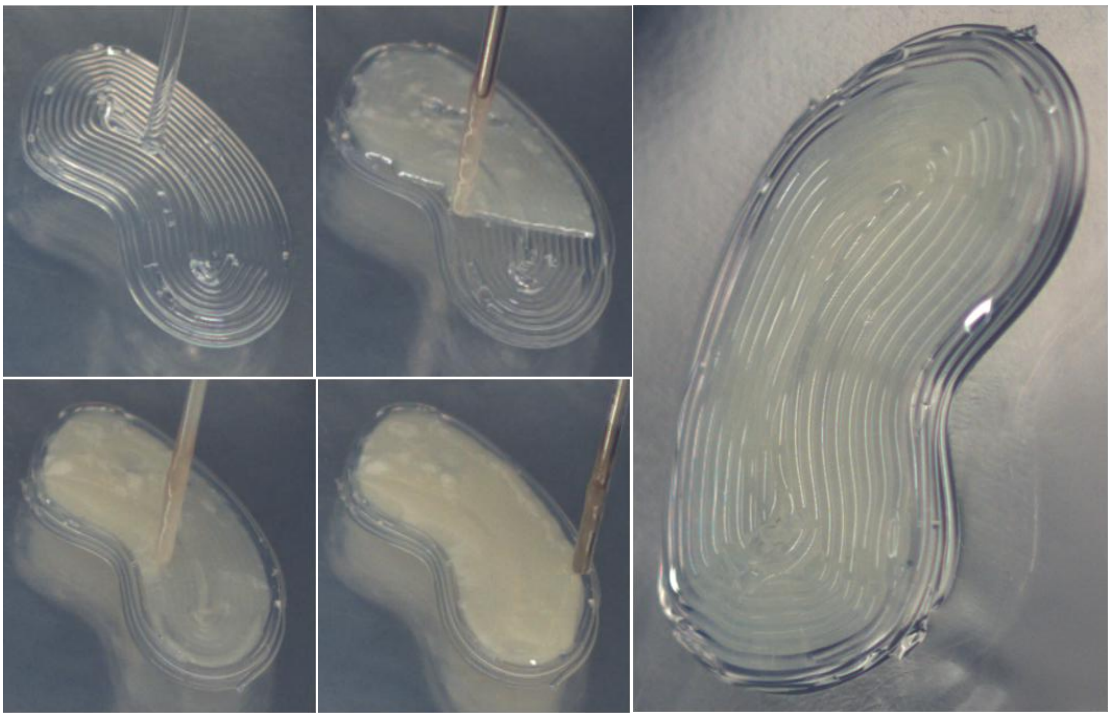

Figure 3.8. Random-shaped printed structure

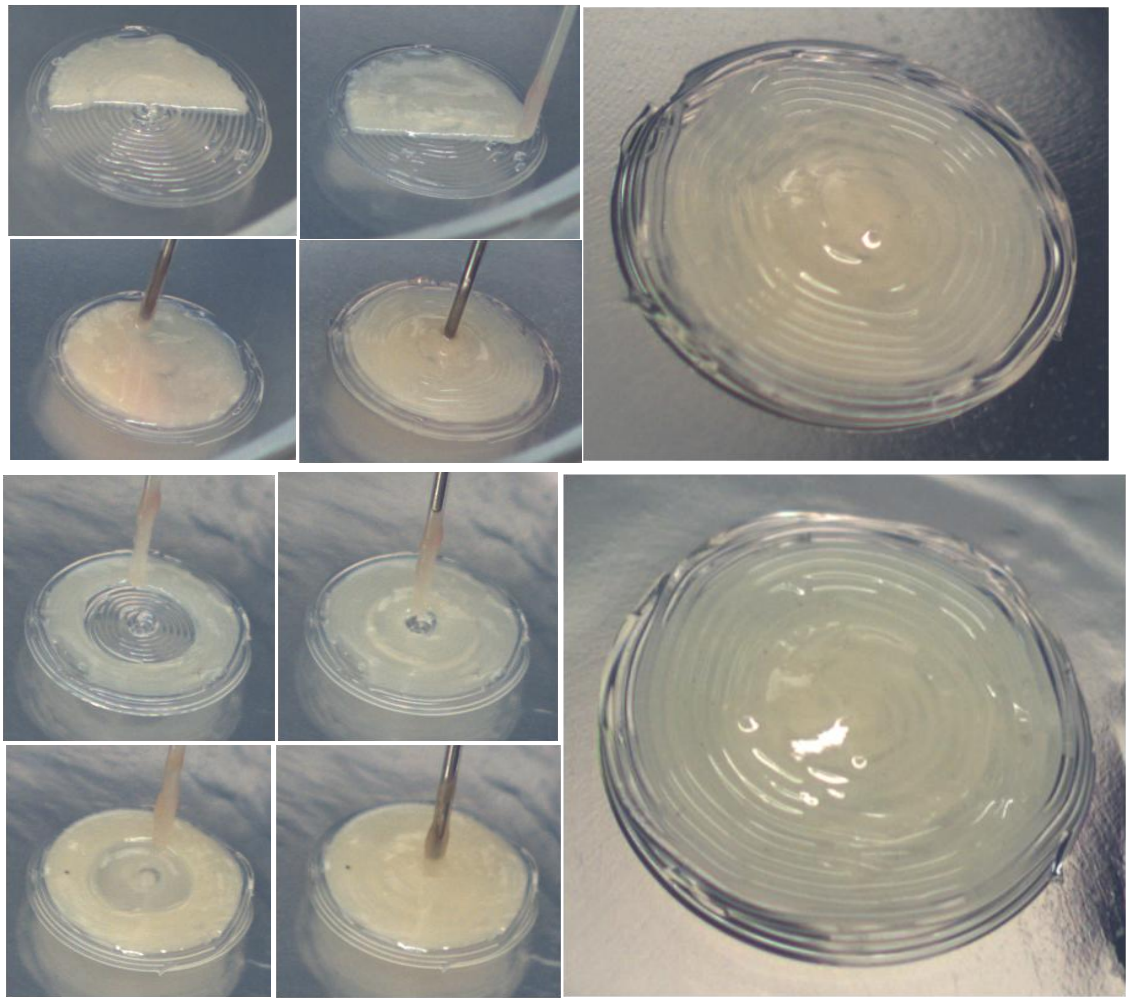

Figure 3.9. Circular shaped printed structures

Cylindrical HUVEC and HDF cell aggregates were 3D bioprinted only with stripe shaped structures; Figure 3.10 illustrates the printing process.

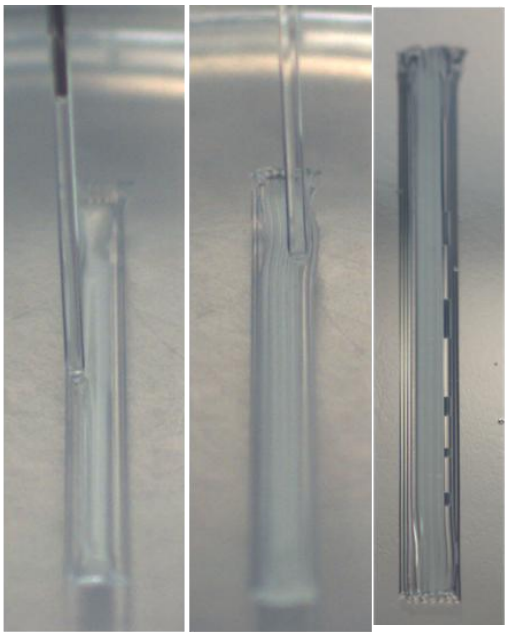

Figure 3.10. Stripe shaped printed structure

3.2.2. Support structure removal and mechanical testing

After a specific time of incubation period, the printed constructs should be transferred into specifically designed bioreactors for further maturation to achieve the necessary mechanical properties for implantation. Therefore, at the end of the incubation period, the printed constructs need to be well-fused and sufficiently sturdy to be handled and transferred into the bioreactors [23]. After 4 or 7 days incubation, the support structures were manually removed and the fused cell structures were tested for transferring with forceps. In well-defined and random-shaped printed structures composed of MOVAS, HUVEC and NIH 3T3 multicellular aggregates, the support structures could not be completely removed as shown in Figure 3.11.

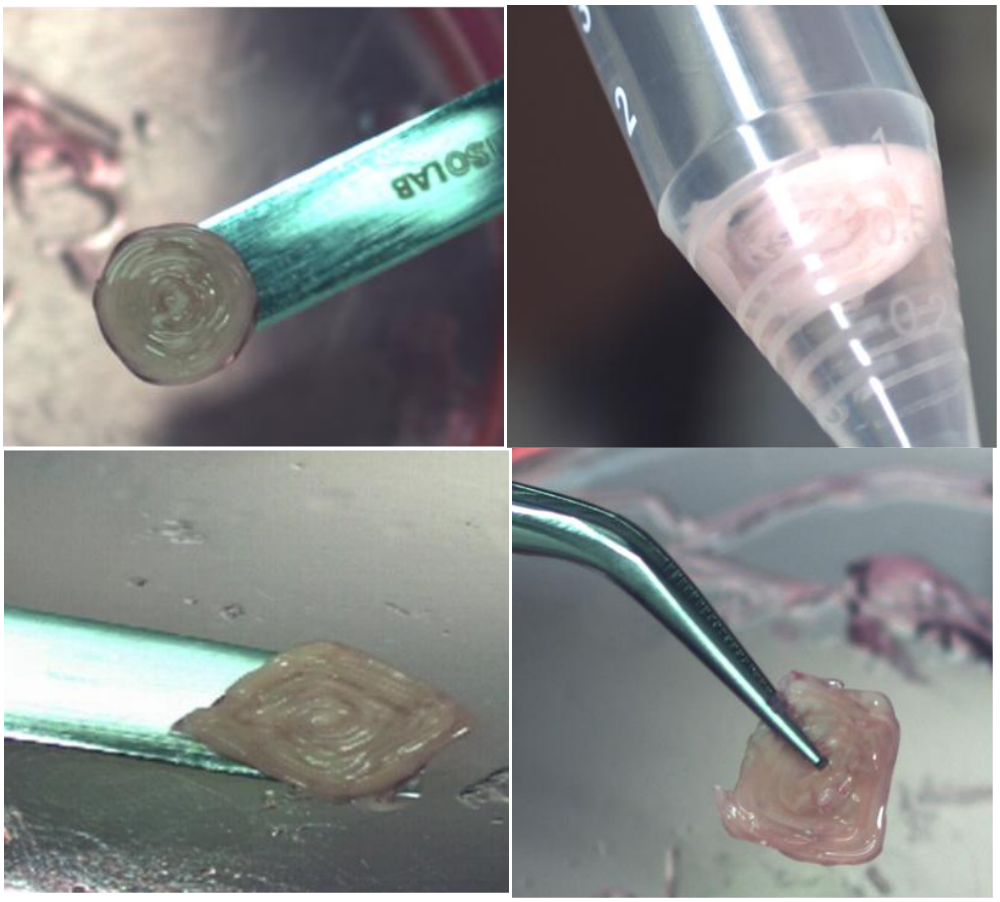

Figure 3.11. Support structure removal in different printed constructs

However, support structures of stripe shaped constructs printed with MOVAS/HUVEC/NIH 3T3 multicellular aggregates or HUVEC/HDF cell aggregates were removed completely and could be transferred with forceps into a falcon filled with PBS as shown in Figure 3.12 and Figure 3.13.

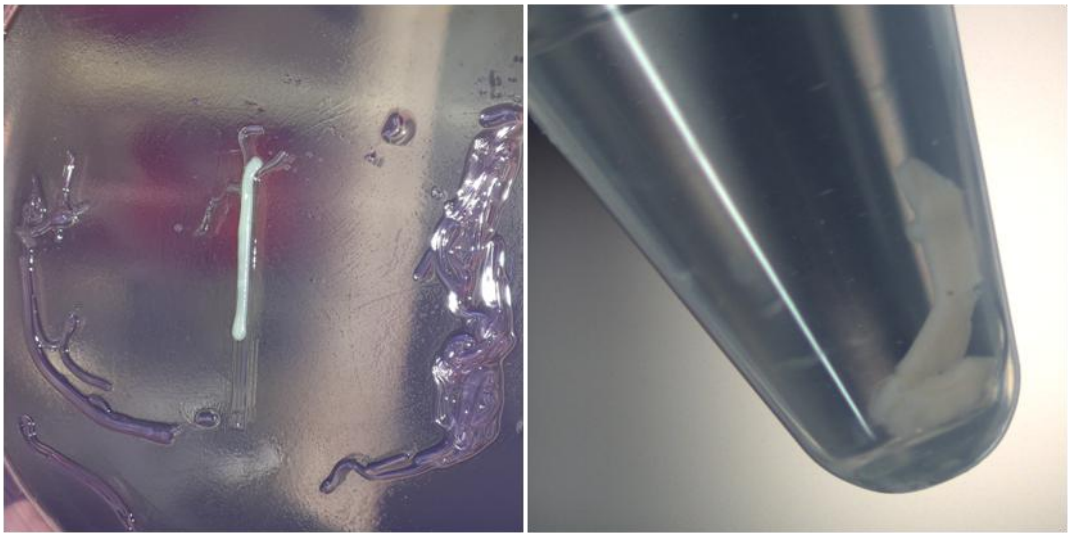

Figure 3.12. Support structure removal of stripe shaped printed construct composed of MOVAS/HUVEC/NIH 3T3 multicellular aggregates

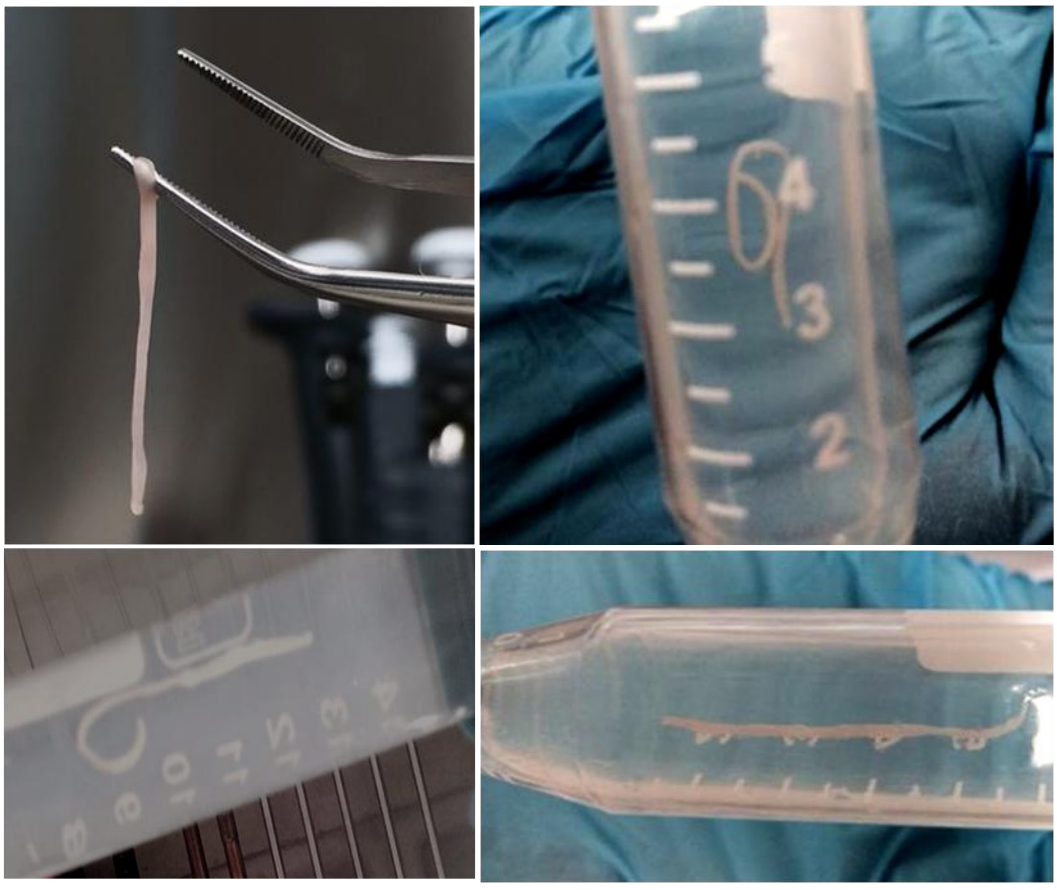

Figure 3.13. Support structure removal of stripe shaped printed construct composed of HUVEC/HDF cell aggregates

3.2.3. Deformation of the printed structures

The printed constructs were observed day by day during the incubation period and pictures were taken with a ruler beside them. Example pictures are shown in Figure 3.14. The length or the area of the printed constructs was measured with ImageJ software program.

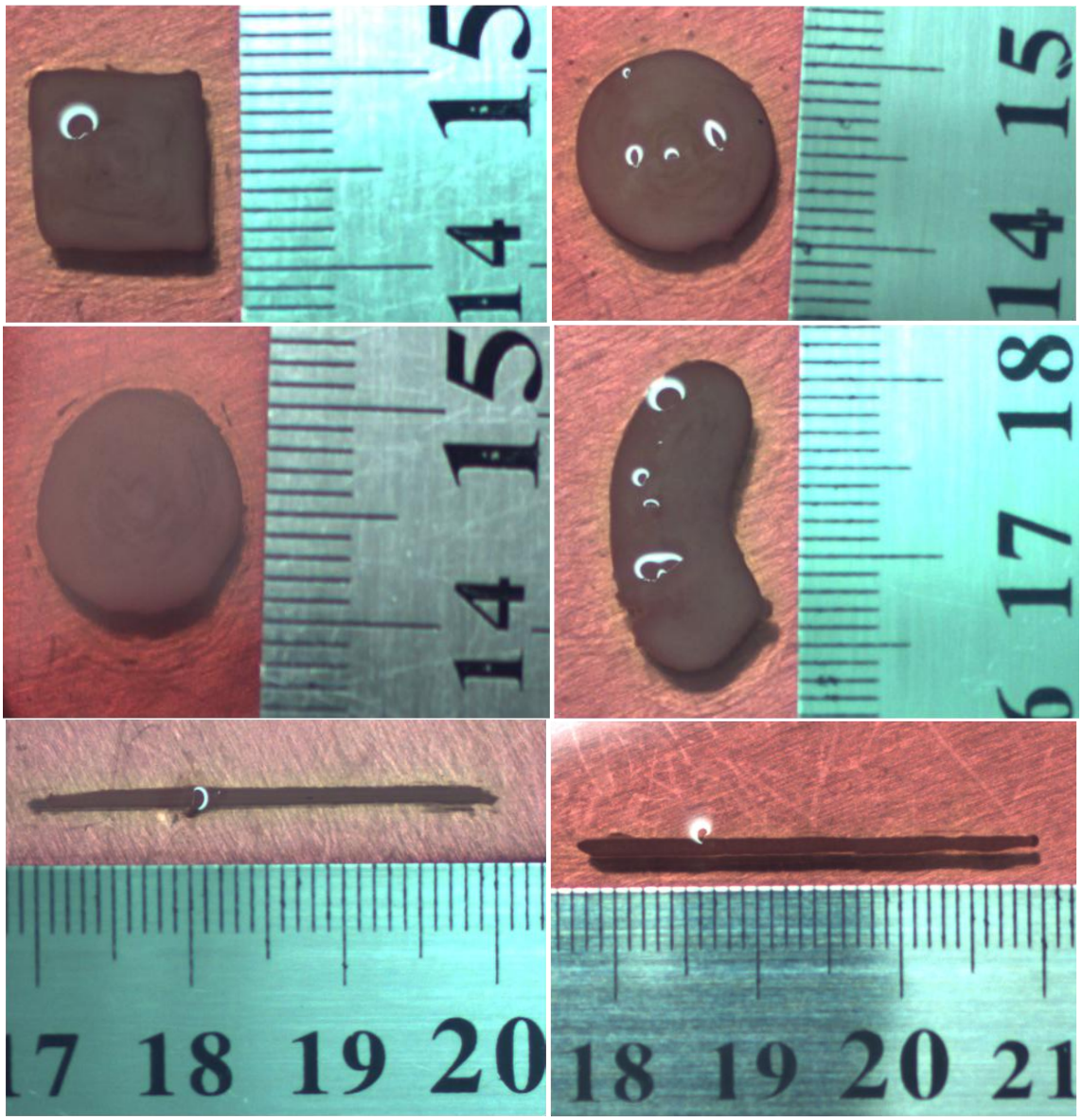

Figure 3.14. Pictures of the printed constructs taken at different days after printing

The size of the printed constructs changed day by day and generally a shrinking between 20% - 38% was observed. The zig-zag patterned and spiral patterned circular shaped structures changed 38% and 35% in size at the end of the 7-days incubation period, respectively (Figure 3.15).

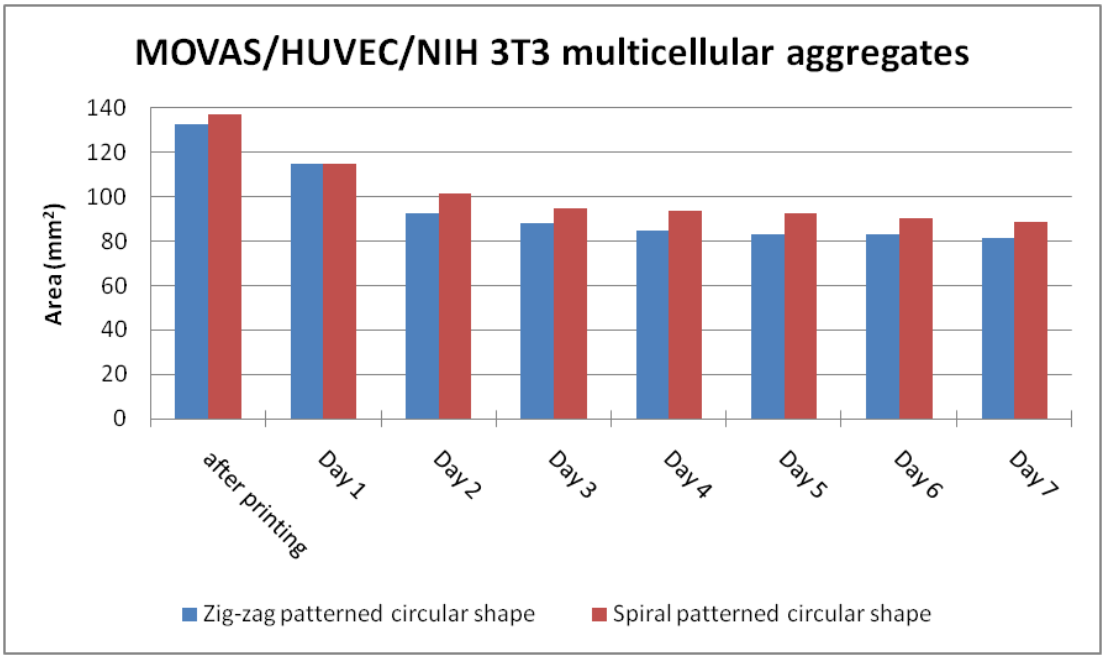

Figure 3.15. Area deformations of zig-zag and spiral patterned circular-shaped printed constructs

After the 7-days incubation, the area of the rectangular shaped structure decreased by 28% (Figure 3.16), while the random-shaped structure changed 24% (Figure 3.17) after 10 days incubation in comparison to its size after printing.

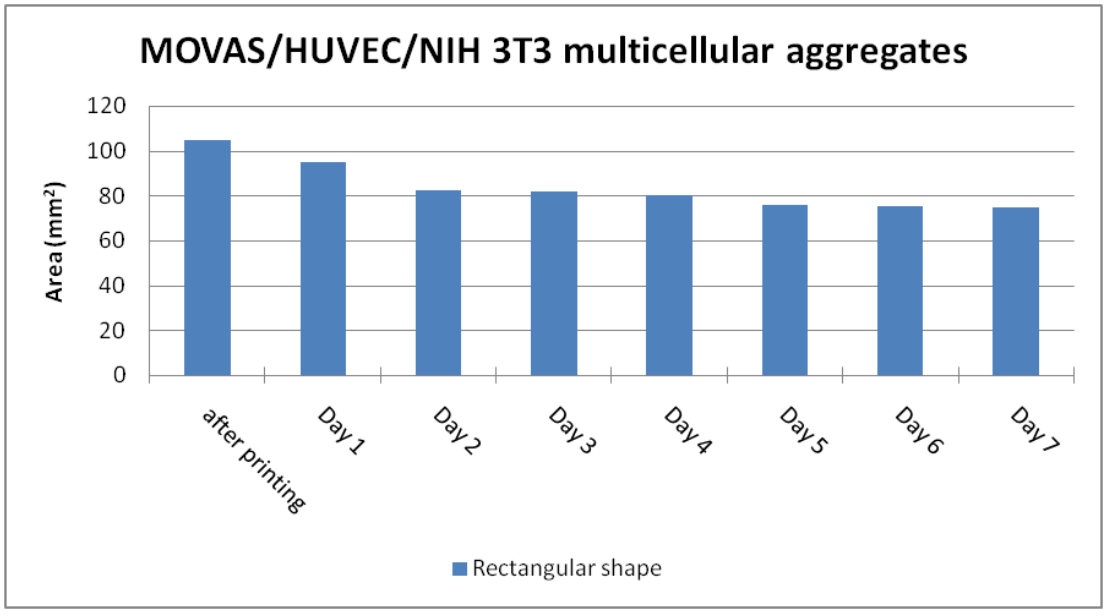

Figure 3.16. Area deformation of rectangular shaped printed construct

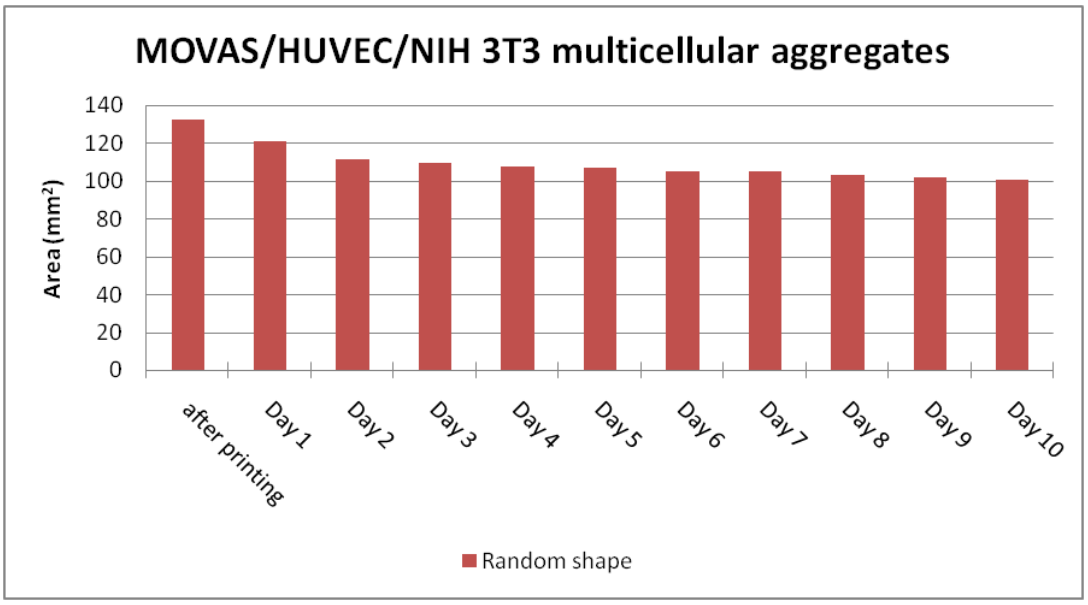

Figure 3.17. Area deformation of random-shaped printed construct

On the other hand, the stripe shaped structure composed of MOVAS/HUVEC/NIH 3T3 multicellular aggregates shrank 35% after 7 days incubation. However, the similar drastic change was not observed in the stripe shaped structure composed of HUVEC/HDF cell aggregates as Figure 3.18 shows. Their length decreased by 5% and 16% after 3-days and 7-days incubation periods, respectively.

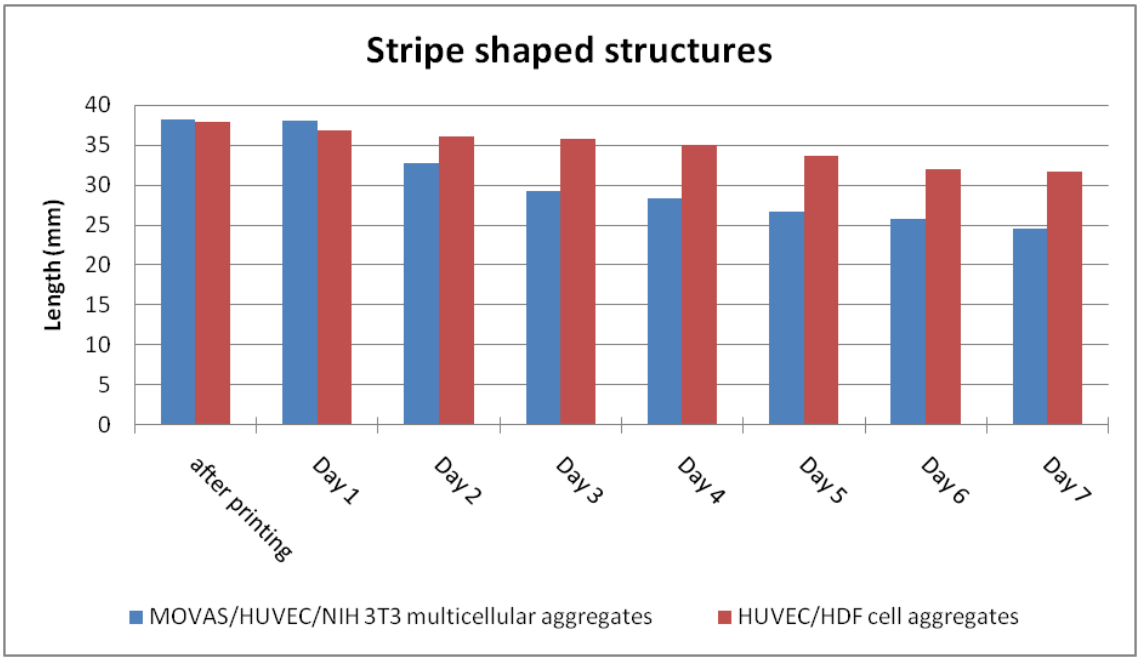

Figure 3.18. Length deformation of stripe shaped printed constructs

3.2.4. Visualization of the cell viability and fusion

After the printing process, the cylindrical multicellular aggregates fused within 2-4 days [23]. To study the fusion process more in detail, the cells are stained with either green or red fluorescence dyes and printed as cylindrical multicellular aggregates based on the developed stripe-shaped model in Figure 3.5 and Figure 3.6. The fusion of the printed cell aggregates was examined 3 days after printing using an Olympus IX70 fluorescent microscope. The fusion of alternate sequences of green and red cylinders is shown in Figure 3.19 and reveals a sharp fusion boundary with little intermingling, which confirms earlier findings [23].

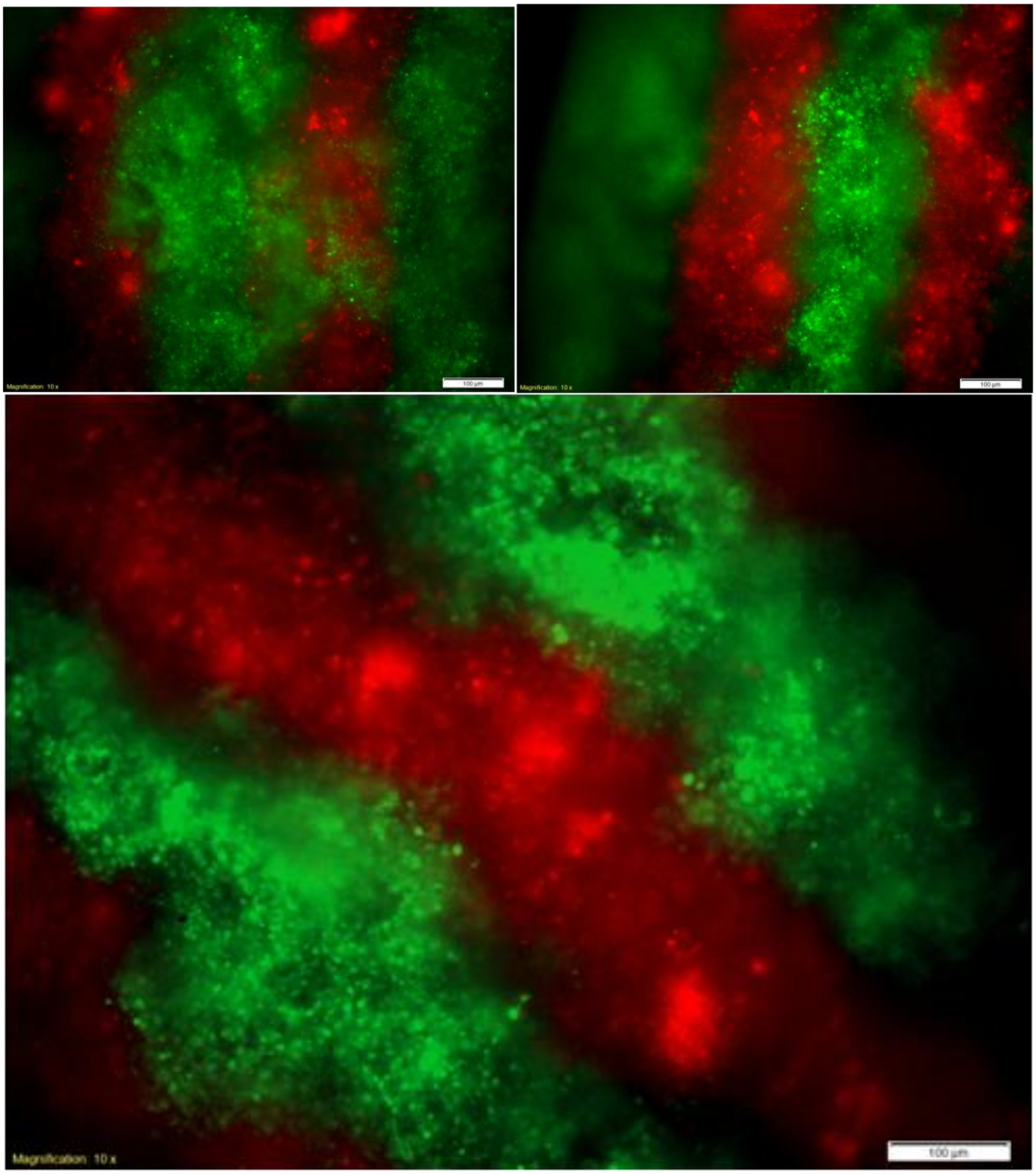

Figure 3.19. MOVAS/HUVEC/NIH 3T3 multicellular aggregates fusion 3days after printing

The cell viability of MOVAS/HUVEC/NIH 3T3 stripe-shaped multicellular aggregates (Figure 3.5 and Figure 3.6) after printing was evaluated using trypan blue stain. The live/dead cell counting under the optical microscope was repeated twice by taking the cell samples randomly resulting in 95% and 97% cell viability, respectively.

Additionally, the cell viability of MOVAS/HUVEC/NIH 3T3 stripe-shaped multicellular aggregates and HUVEC/HDF stripe-shaped cell aggregates (Figure 3.5 and Figure 3.6) after printing was determined using a Live/Dead assay Kit. Live/Dead assay is a convenient discrimination method between live and dead cells. Once the cells are stained, they can be visualized by fluorescence microscopy using a band-pass filter. Calcein is a green fluorescent dye to stain live cells, while PI is a cell non-permeable red fluorescent dye to stain dead cells. The number of live and dead cells was counted by ImageJ software using at least 5 images from arbitrary different areas [22].The cell viability of both MOVAS/HUVEC/NIH 3T3 multicellular aggregates and HUVEC/HDF cell aggregates after printing were 97% (Figure 3.20 and Figure 3.21). This high cell viability corresponds with the result of trypan blue cell viability assay.

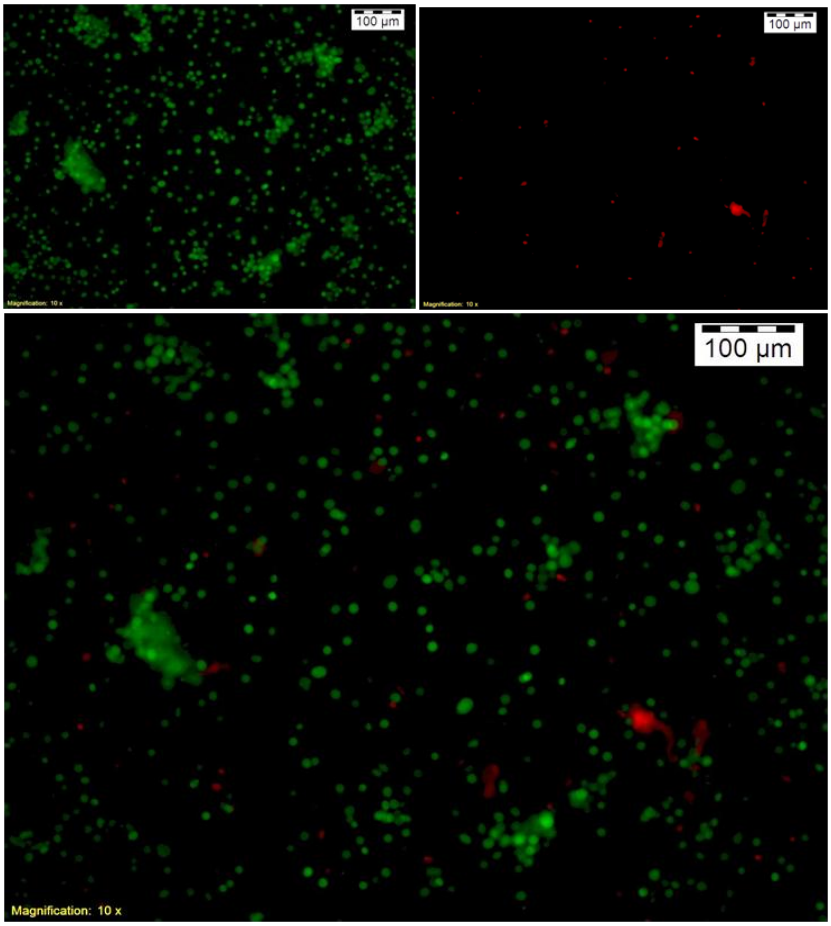

Figure 3.20. Fluorescence microscopy pictures of HUVEC/HDF cell aggregates after printing

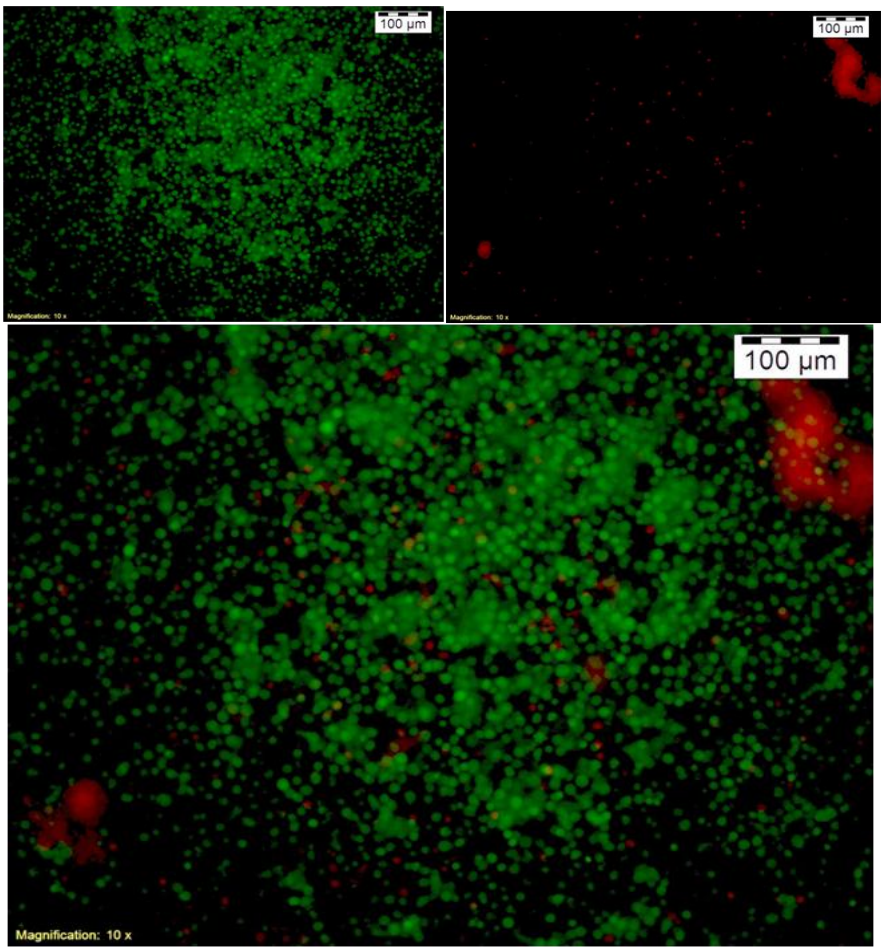

Figure 3.21. Fluorescence microscopy pictures of
MOVAS/HUVEC/NIH 3T3 multicellular aggregates after printing

The cell viability after 3 and 7 days was evaluated also using the Live/Dead assay Kit (Figure 3.22 - Figure 3.25). The cell viability of MOVAS/HUVEC/NIH 3T3 multicellular aggregates and HUVEC/HDF cell aggregates after 3 days incubation were 96% and 95%, respectively. The cell viability of the printed cells decreased to 94% and 92% after 7 days incubation for MOVAS/HUVEC/NIH 3T3 multicellular aggregates and HUVEC/HDF cell aggregates.

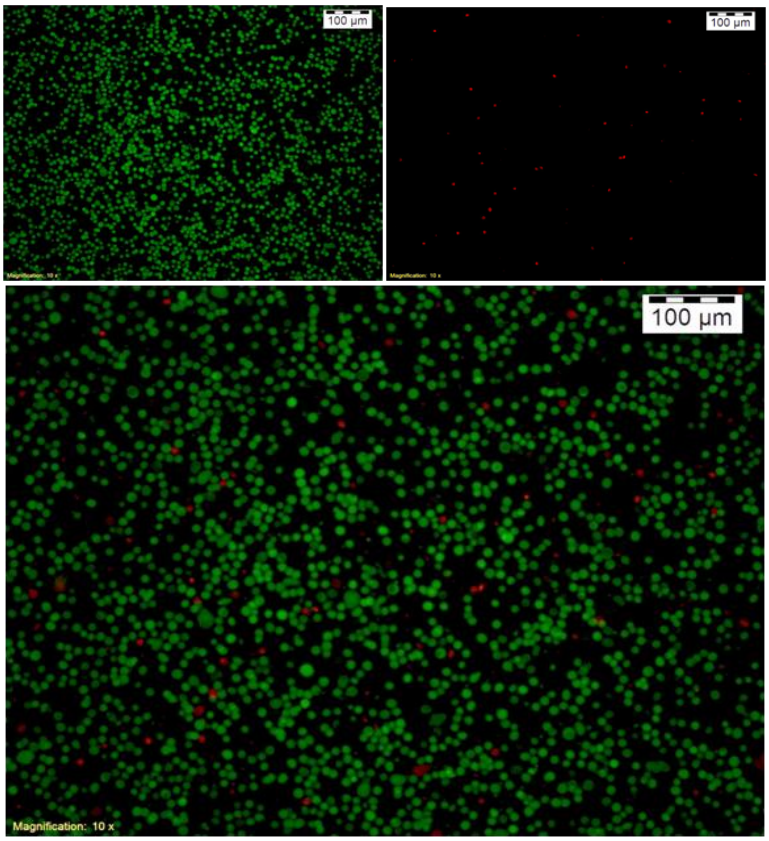

Figure 3.22. Fluorescence microscopy pictures of HUVEC/HDF cell aggregates after 3 days incubation

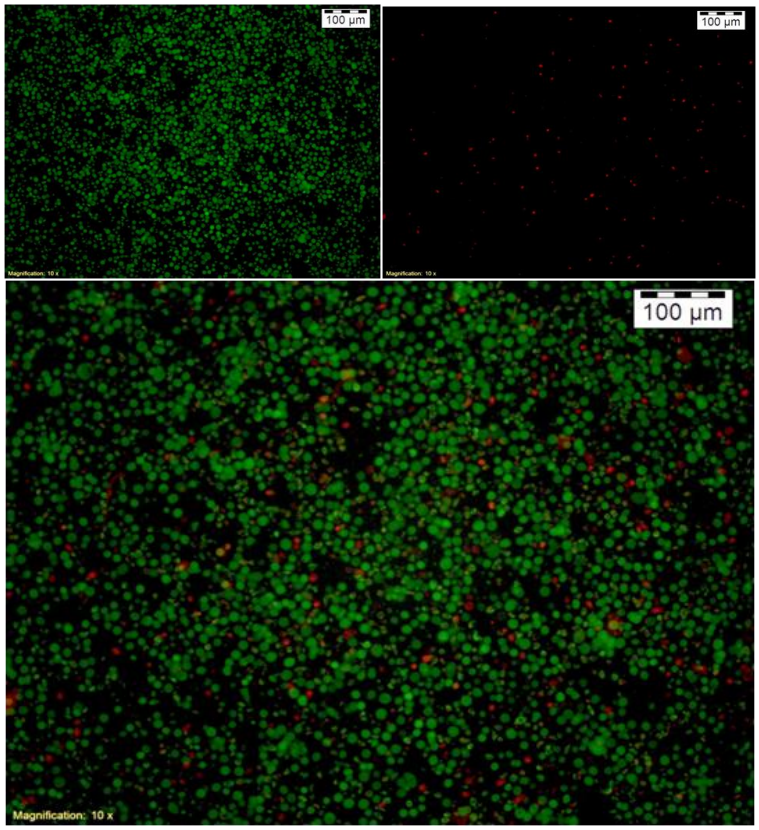

Figure 3.23. Fluorescence microscopy pictures of MOVAS/HUVEC/NIH 3T3 multicellular aggregates after 3 days incubation

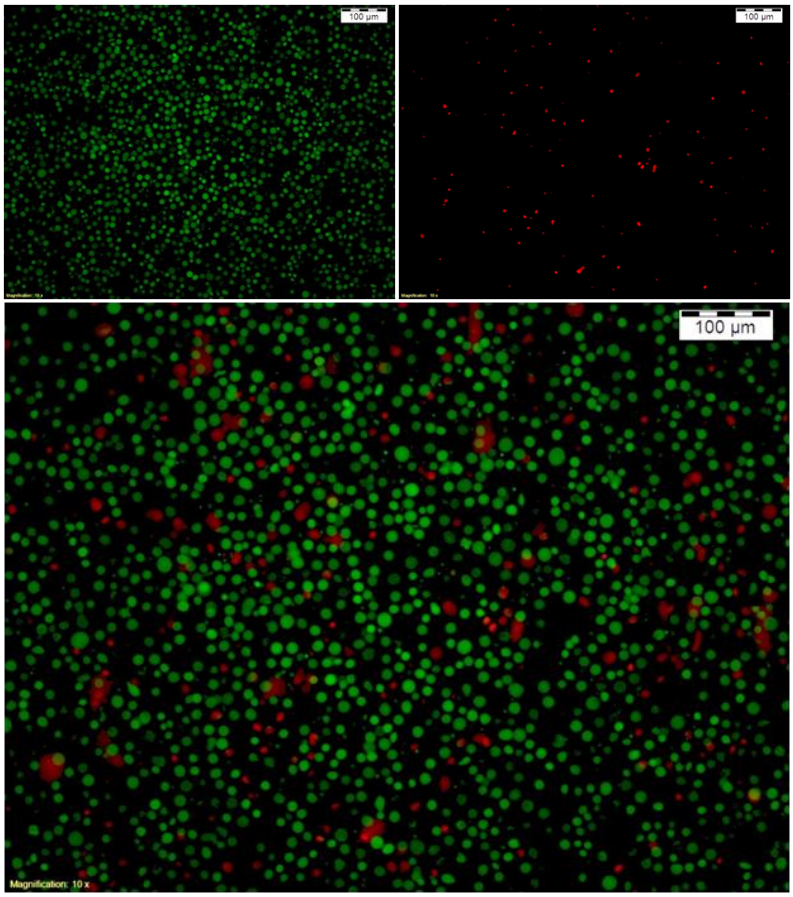

Figure 3.24. Fluorescence microscopy pictures of HUVEC/HDF cell aggregates after 7 days incubation

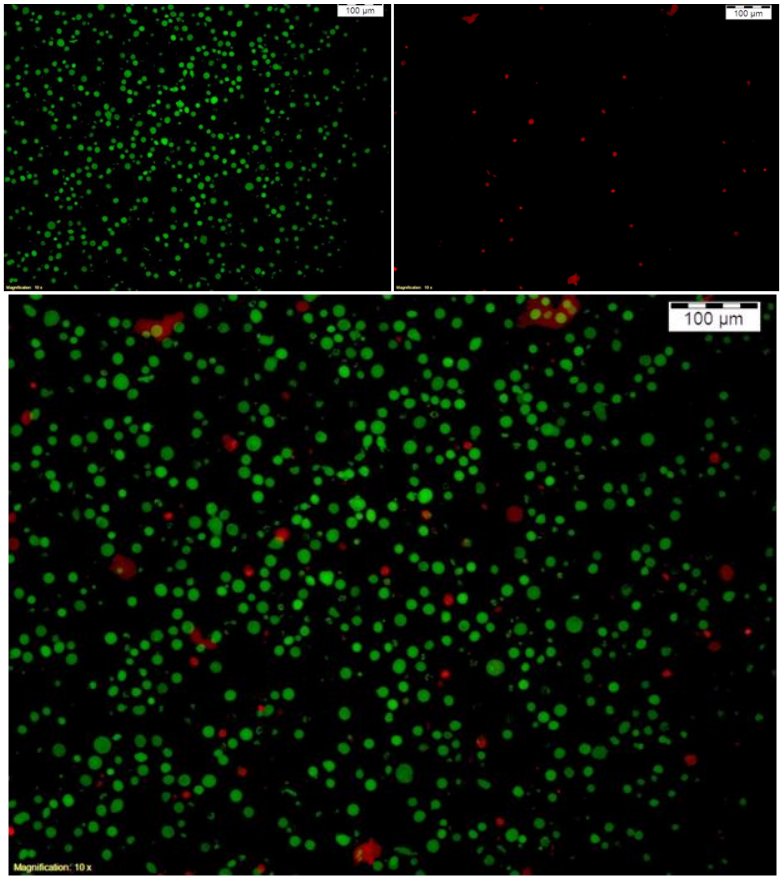

Figure 3.25. Fluorescence microscopy pictures of MOVAS/HUVEC/NIH 3T3 multicellular aggregates after 7 days incubation

The cell viabilities of different cell aggregates are compared based on the incubation time and it is shown in Figure 3.26. These results reinforced that the used 3D bioprinter, the selected operating conditions and applied cellular bioink preparation method are conducive to preserve the cell viability.

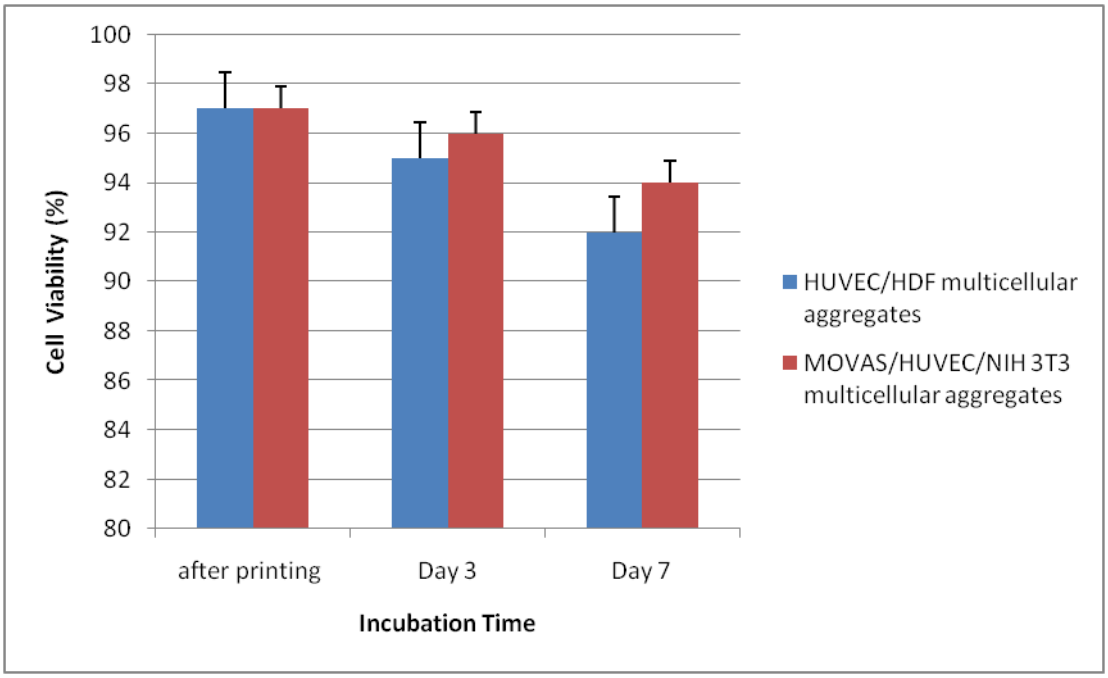

Figure 3.26. Cell viability of different cell aggregates

3.3. Conclusion

Multicellular cell aggregates are 3D bioprinted based on computer-aided semi-continuous and, interconnected tool-path planning methodologies. The printed constructs having different shapes deformed during the incubation period (up to 10-days). It is remarkable that the stripe shaped constructs composed of HUVEC/HDF cell aggregates had a small deformation percentage and were sufficiently sturdy to be handled and transferred. On the other hand, MOVAS/HUVEC/NIH 3T3 multicellular aggregates fused within 3 days, which corresponds to earlier studies [23, 24]. The cell viability upon implementation was high (97%) showing that the cellular bioink preparation method is successful in comparison to other studies in literature. For instance, the 3-day post-printing 3T3 fibroblast cell viability of inkjet printed scaffold-free cellular tubes has been found around 82%.It seems that multicellular aggregates composed of human cells have better mechanical properties. This result confirms also

earlier vascular tissue engineering studies. Blood vessels composed of human smooth muscle, fibroblast and endothelial cells have been fabricated based on cell sheet technology and had high burst strength [27, 30]. Therefore, as a future study, multicellular cell aggregates composed of human aortic smooth muscle cells, HUVEC and HDF cells should be 3D bioprinted in order to obtain mechanically stronger structures which might be building blocks of large and complex tissues.

CHAPTER 4

4. MODELING OF DIRECT CELL PRINTING

4.1. Problem definition

In extrusion based bioprinting processes, biomaterial concentration, loaded cell viscosity, nozzle pressure, and nozzle diameter are determinant parameters for semi-continuous deposition of cylindrical cell aggregates and hydrogel biomaterials. If the cell suspension viscosity is not high enough, drop formation occurs at the end of the capillary and drops initially climb the outer walls of the capillary due to the surface tension as shown in Figure 4.1 [38]. Therefore, a sufficiently high viscosity is required for the cell suspension to overcome surface tension-driven droplet formation and to form continuous filaments.

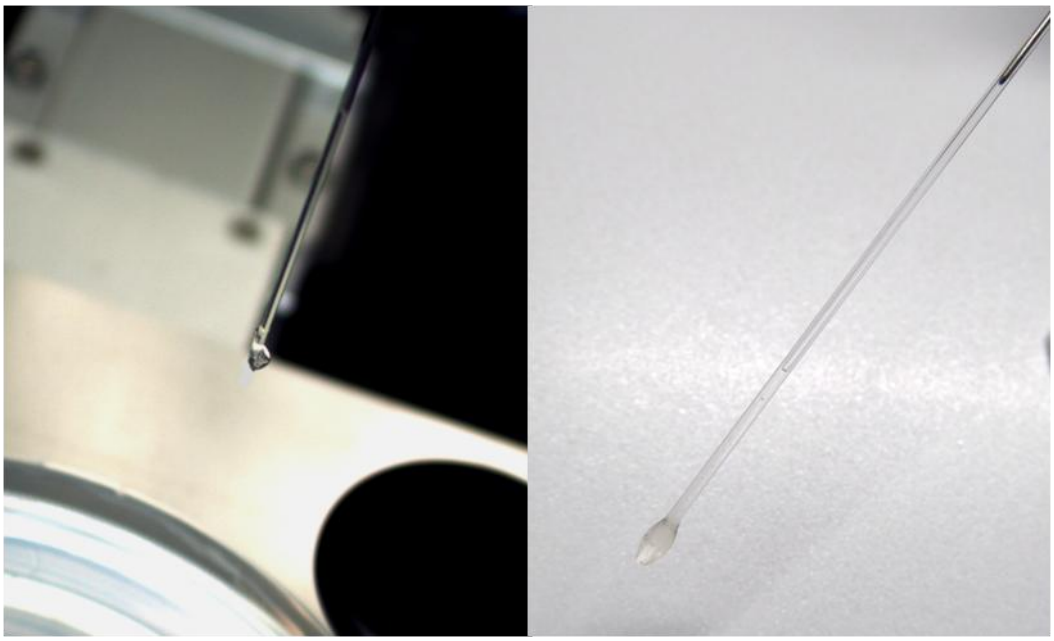

Figure 4.1. Drop formation at the end of the capillary

The fluid-flow behavior of cell suspensions is investigated in order to determine their rheological properties [39-42]. Various mechanical testing methods have been developed including micropipette aspiration, centrifugal force, compression loading, substrate distention methods, and methods based on fluid shear stress [43]. The mechanical behavior of cell aggregates corresponds mostly to visco-elastic materials or non-Newtonian fluids [42]. The cells are spherical when suspended in a culture medium and revealed a shear-thinning behavior based on the work with red blood cells suspensions [40]. Therefore, cell suspension can be considered monodisperse hard-sphere suspension.

In order to increase the viscosity of the cell suspension in the capillary, cell aggregates can be compressed by pushing down the piston while removing a specific amount of medium (Figure 4.2). The compression ratio is directly related to the viscosity of cell suspension and their relationship should be calculated for a successful semi-continuous extrusion.

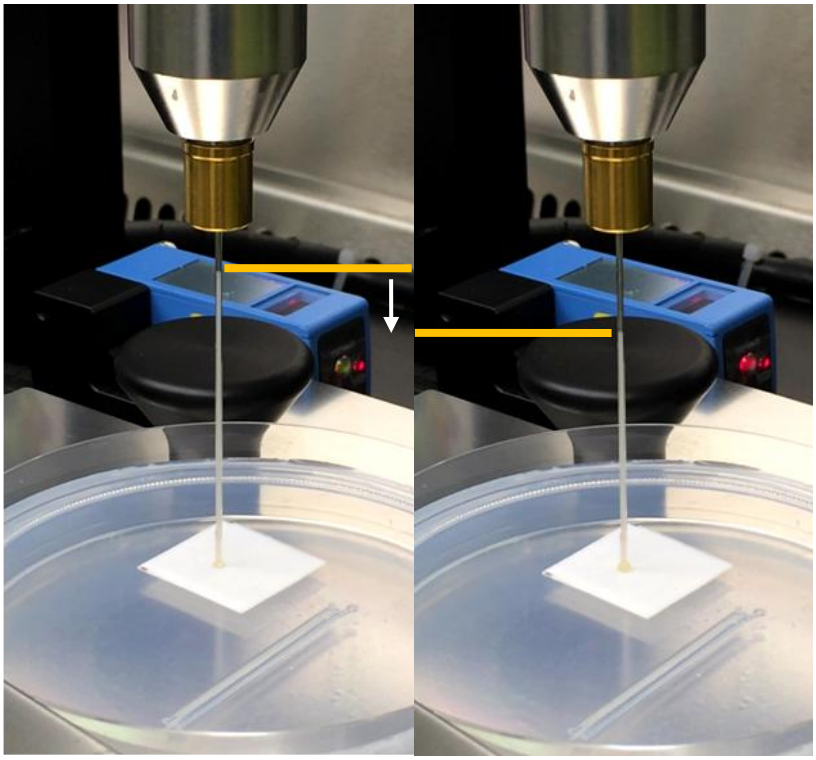

Figure 4.2. Compression of cell aggregates

4.2. Young-Laplace Equation

The interfacial shape of the drop is characterized by the pressure according to the Young-Laplace equation. The Laplace pressure is the pressure difference between the inside and the outside of a curved surface. The pressure difference is caused by the surface tension of the interface between liquid and gas. Cellular aggregates form a spherical shape because their pressure is larger than the ambient atmospheric pressure due to the surface tension. Therefore, the essential pressure to overcome the surface tension can be predicted using the following equation [44]:

$$\Delta p = \alpha \left(\frac{1}{R_1} + \frac{1}{R_2} \right) \quad \text{(Eq. 4.1)}$$

where α is the surface tension, R_1 and R_2 are the radii of the curvature. Δp is the pressure difference to overcome the surface tension in addition to the pressure needed to overcome the external atmospheric pressure. For spherical drop shapes, the radii of the curvature are equal (R_1=R_2) and the equation simplifies to:

$$\Delta p = \frac{2\alpha}{R} \quad \text{(Eq. 4.2)}$$

4.3. Krieger and Doughtery Equation

The viscosity of flowing suspensions depends on the shear rate, and the characteristics of the continuous phase and the discrete phase. Generally, the viscosity of the suspension (η) is directly proportional to the liquid's viscosity (η_o), which might be Newtonian or non-Newtonian. Then, the most rheological models can be described in terms of the relative viscosity of the suspension (η_r) as:

$$\eta_r = \eta / \eta_o \quad \text{(Eq. 4.3)}$$

At high particle concentrations, the relative viscosity of hard-sphere suspensions is expressed by the semi-empirical equation of Krieger and Doughtery [45, 46]:

$$\eta_r = \frac{\eta}{\eta_o} = \left(1 - \frac{\emptyset}{\emptyset_m} \right)^{-[\eta]\emptyset_m} \quad \text{(Eq. 4.4)}$$

where $\emptyset$, $\emptyset_m$ and $[\eta]$ are the volume fraction, the maximum packing fraction and the intrinsic viscosity of the particles, respectively. Theoretically, $[\eta]$ depends on particle shape and being 2.5 for rigid spherical shapes [45]. Maximum volume fraction $\emptyset_m$ changes usually between 0.64 - 0.74 for solid spheres in a face-centered-cubic crystal depending on cell elasticity or their compactness. The value of $\emptyset_m$ for spherical cells can be assumed to be 0.65 based on the rheological study with Chinese Hamster Ovary cells (CHO). η_o is the viscosity of the medium in our case and has the value 0.0014 Pa.s [40].

The capillary can be considered as a cylindrical pipe, where the radius of the pipe is R and the length is L_1 which corresponds to the length of cell suspension aspirated in the capillary. The outer and the inner diameters of the capillary used in our 3D bioprinter are 500 μm and 450 μm, respectively. The length L_1 is taken 5 cm in the following calculations.

In order to calculate the relative viscosity using Krieger and Doughtery equation, volume fraction (∅) of the cells in the suspension should be determined. In a study, the surface tension of human umbilical smooth muscle cell (HUSMC) aggregates is evaluated and 300-micron diameter aggregates composed of 12,000 cells have a surface tension of 279 mN/m. As scanning electron microscopy image shows, cell aggregates have a spherical shape (Figure 4.3) [39, 41].

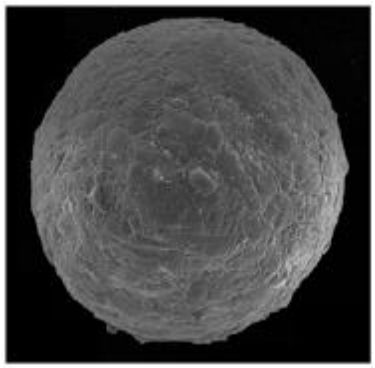

Figure 4.3. Scanning electron microscopy image of 300-micron diameter HUSMC aggregates

The volume of a cell aggregate with a 300 μm diameter value is calculated using sphere volume formula:

$$V_{agg} = \frac{4}{3}\pi R^3 = 0.014\ mm^3 \quad \text{(Eq. 4.5)}$$

Based on the information that 300-micron diameter HUSMC aggregate contains 12,000 cells, single cell volume and radius are evaluated as 1178.1 μm^3 and 6.55 μm, respectively.

Based on our experiments, HUSMC suspension aspirated 5 cm long in the 500-micron diameter capillary contains $4x10^6$ smooth muscle cells. Accordingly, total cell volume in the capillary is 4.712 mm^3.

Capillary volume is calculated using the volume formula of a cylinder (D_i=450 μm):

$$V_c = \frac{\pi D_i^2}{4} L_1 = 7.952\ mm^3 \quad \text{(Eq. 4.6)}$$

Therefore, volume fraction (∅) of the cells in the suspension is obtained as follows:

$$\text{volume fraction } (\emptyset) = \frac{total\ \ cell\ \ volume\ \ in\ the\ capillary}{capillary\ \ \ volume} = \frac{4.712\ mm^3}{7.952\ mm^3} = 0.593 \quad \text{(Eq. 4.7)}$$

The viscosity of the cell suspension η_{wall} can be calculated by combining Krieger and Doughtery equation with Eq. 4.6 and Eq. 4.7 resulting in the following general formula:

$$\frac{\eta_{\text{wall}}}{\eta_0} = \left(1 - \frac{\frac{total\ \ cell\ \ volume\ \ in\ the\ capillary}{capillary\ \ \ volume}}{\emptyset_m}\right)^{-[\eta]\emptyset_m} =$$

(Eq. 4.8)

$$= \left(1 - \frac{\frac{total\ \ cell\ \ volume\ \ in\ the\ capillary\ *4}{\pi * D_i^2 * L_1}}{\emptyset_m}\right)^{-[\eta]\emptyset_m}$$

Finally, viscosity of the cell suspension (η) is calculated with Krieger and Doughtery equation:

$$\frac{\eta_{wall}}{\eta_o} = \left(1 - \frac{\emptyset}{\emptyset_m}\right)^{-[\eta]\emptyset_m} = \frac{\eta}{0.0014\ Pa.s} = \left(1 - \frac{0.593}{0.65}\right)^{-2.5*0.65} = 51.6 \quad \text{(Eq. 4.9)}$$

$$\eta = 0.07224\ \text{Pa. s}$$

4.4. Capillary Flow of a Power-Law Fluid

In capillary rheometry, the shear viscosity of a fluid can be determined by shear rate. The pressure drop across the capillary with radius R and length L is Δp and the flux of the fluid through the capillary is Q. Navier-Stokes equation with cylindrical coordinates is as follows[47]:

$$\rho\left(\frac{\partial v_z}{\partial t}+v_r\frac{\partial v_z}{\partial r}+\frac{v_\theta}{r}\frac{\partial v_z}{\partial \theta}+v_z\frac{\partial v_z}{\partial z}\right)=$$

$$-\frac{\partial p}{\partial z}+\left[\frac{1}{r}\frac{\partial}{\partial r}(r\tau_{rz})+\frac{1}{r}\frac{\partial}{\partial \theta}\tau_{\theta z}+\frac{\partial}{\partial z}\tau_{zz}\right]+\rho g_z \qquad \text{(Eq. 4.10)}$$

We can assume that the flow in the capillary is steady, uni-directional and uniform in z which reduces the Navier-Stokes equation as follows:

$$0=-\frac{\partial p}{\partial z}+\frac{1}{r}\frac{\partial(r\tau_{rz})}{\partial r} \qquad \text{(Eq. 4.11)}$$

This equation may be integrated with respect to R and scale $\frac{\partial p}{\partial z}$ with $\frac{\Delta p}{L}$ to give:

$$\tau_{rz}=\frac{r}{R}\tau_{wall} \qquad \text{(Eq. 4.12)}$$

whereτ_{wall} represents the stress on the wall and is given by $\tau_{wall}=\frac{\Delta pR}{2L}$. The equation for power-law fluid is:

$$\tau_{rz}=k\dot{\gamma}^n \qquad \text{(Eq. 4.13)}$$

where k is a constant and $\dot{\gamma}$ the shear rate. For the capillary flow, the shear rate can be described as:

$$\dot{\gamma}=-\frac{dw}{dr} \qquad \text{(Eq. 4.14)}$$

where*w* is the axial velocity. Substitution of this expression into Eq. 4.13 and then combine it with Eq. 4.12 gives the following equation:

$$-k\left(\frac{dw}{dr}^n\right)=\frac{r}{R}\tau_{wall} \qquad \text{(Eq. 4.15)}$$

Integration of this equation with respect to R gives the axial velocity, w.

$$w = \left(\frac{\tau_{wall}}{kR}\right)^{1/n} \frac{R^{\frac{1}{n}+1} - r^{\frac{1}{n}+1}}{\frac{1}{n}+1} \qquad \text{(Eq. 4.16)}$$

For Newtonian flow with n =1, the structure of the flow is quadratic. In our case, n value of the shear thinning fluid is n<1. Therefore, the flow profile is flatter in the middle and decays faster towards the wall. Near the middle of the capillary, the stress τ is low, and the viscosity μ is high. Near the boundary of the capillary, the stress τ is high, and the viscosity μ is low.

The volume flux of the fluid in the capillary can be expressed as:

$$Q = \int_0^R w 2\pi r dr = w\pi r^2|_0^R - \int_0^R \frac{dw}{dr} \pi r^2 dr \qquad \text{(Eq. 4.17)}$$

$w\pi r^2|_0^R$=0 because the axial velocity is zero at the boundary. Eq. 4.17 can be rewritten as:

$$Q = -\int_0^R \dot{\gamma}\, \pi r^2 dr \qquad \text{(Eq. 4.18)}$$

Based on the Eq. 4.12, the radius is given by $r = \frac{R\tau_{rz}}{\tau_{wall}}$. The integration variable may be changed from the radius R to the stress τ to express the flux through the capillary as follows:

$$Q = -\frac{\pi R^3}{\tau_{wall}^3} \int_0^{\tau_{wall}} \dot{\gamma}\,(\tau)\tau^2 d\tau \qquad \text{(Eq. 4.19)}$$

Differentiation of the above equation with respect to τ_{wall}, shear rate on the wall $\dot{\gamma}_{wall}$ is obtained:

$$\dot{\gamma}_{wall} = -\frac{1}{\tau_{wall}^2} \frac{d}{d\tau_{wall}} \left(\frac{\tau_{wall}^3 Q}{\pi R^3}\right) = -\frac{1}{\pi R^3}\left(3Q + \tau_{wall} \frac{dQ}{d\tau_{wall}}\right) \qquad \text{(Eq. 4.20)}$$

Since the stress on the wall τ_{wall} is linearly proportional to the pressure gradient Δp, Eq. 4.20 can be simplified as:

$$\dot{\gamma}_{wall} = -\frac{1}{\pi R^3}\left(3 + \frac{d \ln Q}{d \ln \Delta p}\right) \qquad \text{(Eq. 4.21)}$$

Therefore, the viscosity on the wall η_{wall} can be described as:

$$\eta_{wall} = \frac{\tau_{wall}}{\dot{\gamma}_{wall}} = \frac{\Delta p R}{2L\dot{\gamma}_{wall}} \quad \text{(Eq. 4.22)}$$

For a Newtonian flow, the value of $\frac{d \ln Q}{d \ln \Delta p}$ =1 and $\dot{\gamma}_{wall} = -\frac{4}{\pi R^3}$. In this case, Eq. 4.22 changes and gives the Hagen-Poiseuille equation for Newtonian flow:

$$\eta_{wall} = \frac{\Delta p \pi R^4}{8L} \quad \text{(Eq. 4.23)}$$

For a shear thinning fluid, $\frac{d \ln Q}{d \ln \Delta p}$ or n should be determined since there is the following relationship:

$$\frac{d \ln Q}{d \ln \Delta p} = \frac{1}{n} \quad \text{(Eq. 4.24)}$$

In order to calculate the shear rate and the viscosity on the wall, shear thinning value $n$of the cell suspension should be determined. The shear rheology of cell suspensions can be described by the power-law model. The viscosity η (Pa.s) vs. shear rate $\dot{\gamma}$ (s^{-1}) data of CHO cells with a 60% volume fraction (∅) is obtained from literature and plotted as shown in Figure 4.4 [40]. 60% volume fraction corresponds to the calculated volume fraction, which is 0.593 %.

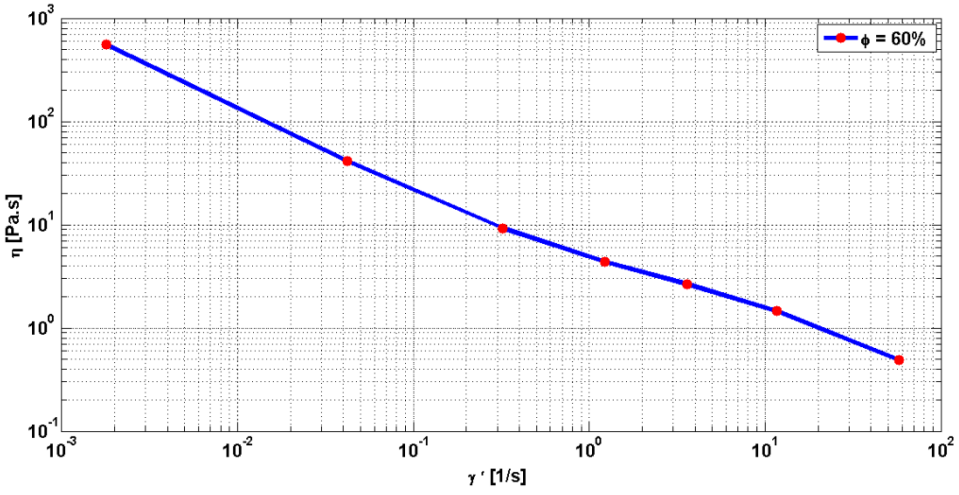

Figure 4.4. Viscosity η (Pa.s) vs. shear rate $\dot{\gamma}$ (s^{-1}) with ∅ =60 %

From the viscosity curve in Figure 4.4, the stress rate (τ) is calculated by τ= η*$\dot{\gamma}$ and stress rate (τ) vs. shear rate ($\dot{\gamma}$) is plotted. The data is fitted with power-law model in order to obtain k and n values. According to the plot in Figure 4.5, k and n values are 5.885 and 0.392, respectively.

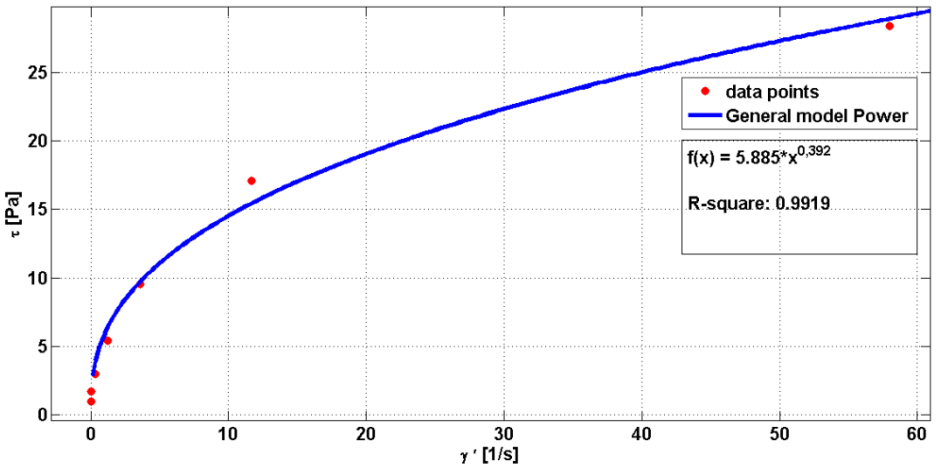

Figure 4.5. Determination of n using Power-law model

Once the n value is obtained, shear rate ($\dot{\gamma}_{wall}$) can be evaluated by combining the equations 4.21 and 4.24 which gives the following equation:

$$\dot{\gamma}_{wall} = -\frac{1}{\pi R^3}\left(3+\frac{1}{n}\right) \qquad \text{(Eq. 4.25)}$$

As Figure 4.1 shows, drop forming from the capillary initially climb to the outer walls of the capillary due to the surface tension. Therefore, for the calculation of the shear rate ($\dot{\gamma}_{wall}$) value, the diameter of the drop is assumed as 520 µm which is a higher value than the outer diameter of the capillary (500 µm). The calculation gives the value 100.53 s^{-1} for shear rate ($\dot{\gamma}_{wall}$) as a result.

The length L_2, which is the length after compression, can be calculated by rewriting Eq. 4.22:

$$L_2 = \frac{\Delta p R}{2\dot{\gamma}_{wall}\,\eta_{wall}} \qquad \text{(Eq. 4.26)}$$

$\Delta p$is calculated using the above explained Young-Laplace Equation (4.2):

$$\Delta p = \frac{2\alpha}{R} = \frac{2*0.279 N/m}{260*10^{-6} m} = 2146\ Pa \qquad \text{(Eq. 4.27)}$$

Combining the Eq. 4.2 and Eq. 4.26 gives the following general formula for L_2 calculation:

$$L_2 = \frac{\alpha}{\dot{\gamma}_{wall}\,\eta_{wall}} \qquad \text{(Eq. 4.28)}$$

Finally, the length L_2 is calculated using Eq. 4.28:

$$L_2 = \frac{\alpha}{\dot{\gamma}_{wall}\,\eta_{wall}} = \frac{0.279\ N/m}{100.53\ s^{-1} * 0.07224\ Pa.s} = 0.0384m = 3.84\ cm \qquad \text{(Eq. 4.29)}$$

4.5. Discussion and Conclusion

According to calculations, 5 cm long L_1 value should be compressed to L_2=3.84 cm resulting in a compression ratio 0.23. In practice, cell aggregates in the capillary are used to be compressed 1 cm to obtain a semi-continuous bioprinting. Therefore, the theoretical value corresponds with our experimental implementation. It should be considered that the rheological parameter values used through the calculations does not belong to the bioprinted cell types in our experiments. However, this theoretical approach offers an insight into the relationship between the viscosity of cell suspension and compression ratio. Accordingly, it can be repeated after obtaining the rheological parameters of the bioprinted cell types. The radius of the drop formed at the end of the capillary was assumed for the determination of the shear rate. In order to be more accurate, the formation and the motion of the drops can be analyzed more accurately using digital imaging processing [38].

On the other hand, the compression of the different cell types during the printing process does not have an adverse effect on cell viability according the cell viability results in the previous chapter. However, the effect of compression on the viability and differentiation should be further examined in case of using the system for stem cell printing. Since the extensional flow at the entrance of the syringe needle can cause an acute death of stem cells, the compression procedure can cause an expectable cell viability decrease [48].

CHAPTER 5

5. 3D BIOPRINTING OF BIOMIMETIC AORTIC VASCULAR CONSTRUCTS

As mentioned in the literature review, many people around the world suffer from cardiovascular diseases which are traditionally treated with autografts and blood vessel transplantations. Recently, valve and vascular tissue engineering studies focus on finding alternative solutions to remove the existing problems of the traditional treatments. Scaffold-free tissue engineering of small-diameter tubular grafts is widely studied in literature. However, there is a lack of research about fabricating scaffold-free biomimetic macrovascular structures.

In this chapter, novel computer-aided algorithms and strategies are developed to model and 3D bioprint a scaffold-free human aortic tissue construct biomimetically. A macro-vascular computer model is first generated biomimicking a real human aorta model directly from medical images. Three-dimensional bioprinting path planning and parameter optimization are developed with the proposed 'Self-Supporting' model. Live mouse embryonic fibroblast (MEF) and human dermal fibroblast cells (HDF) aggregates, and support structures (hydrogels) are 3D bioprinted layer-by-layer according to the developed computer models to form biomimetic aortic vessel structures.

5.1. Materials and Methods

Again, the NovoGenMMX^{TM} Bioprinter (Organovo) (Figure 1.1) is used to bioprint cell aggregates and support structures. As before, thermo-reversible, bioinert NovoGel is used for printing the support structures. The base plate, on which the printing process is

performed, and NovoGel are prepared according to the procedures explained in the previous chapter.

5.1.1. Cell culture and bio-ink preparation

Early passage primary mouse embryonic fibroblast (MEFs isolated from C57BL/6 strain) cells were immortalized using SV40 Large T genome using standard protocols[49]. Cells were cultured at 37 ^{o}C and under 5% CO_2 using DMEM culture medium (Sigma, Germany) supplemented with 10% FBS (Biochrom KG, Germany), 1% Penicillin-Streptomycin (Biological Industries, Israel), 1% L-glutamin (Biological Industries, Israel), 55 μM β-mercaptoethanol (Sigma, Germany) and 0.8 μg/ml puromycin (Sigma, Germany). Subconfluent and low passage cultures were used for this study[49].

Immortalized MEF cells were cultured in 15 cm-diameter culture dishes. Cells were detached from the culture plate using two different approaches. Cells were either detached using 0.1% trypsin (Biological Industries, Israel) for 10 minutes (Exp1), or 2.5 mM EGTA (ethylene glycol-bis(2-aminoethyl ether)-N,N,N´,N) (Idranal VI, Fluka, Germany) in PBS. Following detachment, trypsin or EGTA was neutralized using serum containing medium. Following detachment, cells were centrifuged at 200 g and supernatant was discarded. The cell pellet was resuspended to obtain 10 x 10^6 cells / 20 ml medium incubated at 37°C in 15 ml-conical tubes under rotation (PTR-30 Grant-Bio rotator, U.K). Following pelleting, cells were resuspended in 1 ml medium and transferred into 1.5 ml Eppendorf tubes and centrifuged again (1000 g).

Human dermal fibroblast (HDF, generously provided by Yeditepe University, Turkey) cells were cultured at 37°C in 5% CO_2 using Dulbecco's Modified Eagle's Medium (DMEM, Sigma, Germany) supplemented with 10% fetal bovine serum (FBS, Sigma, Germany), 1% Penicillin-Streptomycin (Sigma, Germany).

HDF cells were cultured in tissue culture flasks. Following the removal of the culture medium from culture flasks, cells were washed with PBS and detached by using cells scrapers. Following the detachment step, cells were centrifuged at 1100 RPM for 5 minutes, then supernatant was discarded thus a cell pellet is obtained. Once the cell pellet was obtained, it was resuspended in 1 mL of culture medium and transferred into T25 tissue culture flasks (TPP, Germany) containing 6 mL culture medium. T25 tissue

flasks were incubated at 37°C and 5% CO_2 on an orbital shaker (using IKA, KS 130 basic, Germany) and shaken at 160 rpm for 60 minutes. Then, the cells are collected and centrifuged at 1100 RPM. After removing the supernatant, the cell pellet was resuspended in a 1 mL medium and transferred into 1.5 mL Eppendorf tubes and centrifuged again at 1000 g (≈3000 RPM) for 5 minutes to form a dense cell pellet.

After discarding the supernatant, cell pellets in the Eppendorf tubes were non-formed multicellular aggregates to be aspired into capillaries for formation of cylindrical multicellular aggregates (bio-ink) for semi-continuous bioprinting as explained in Chapter 3 according to the developed algorithms.

5.2. 3D Bioprinting of aortic vascular structure using novel self-supporting method

A roadmap of the proposed approach is presented in Figure 5.1. Novel computer aided algorithms are developed in order to 3D bioprint cell and support structures for scaffold-free macro-vascular tissue engineering. Rhino3D using Rhinoscript language is used as a CAD software package for the generation of the developed algorithms. The tool path design and 3D printing parameters are optimized for an anatomically correct 3D printing of the human aorta. Briefly, the method for biomodeling and bioprinting of aortic vascular structure using self-support includes as follows. More details can be found in [49]:

- Medical images obtained from computer tomography (CT) or magnetic resonance imaging (MRI) is used to obtain the geometric and topological information of the targeted aorta. The main abdominal aorta model from a sample MRI data is used to highlight the proposed methods' capabilities for 3D bioprinting of macrovascular structures.

- In order to obtain 3D computer models of the aortic tissue, MRI images are segmented using the Mimics software [50]and converted into 3D mesh model such as stereolithography (STL) model. The STL models are generated by tessellating the outer surface of the mesh model with triangles. Therefore, for tool path planning as well as for optimization of 3D bioprinting, the resultant STL model of aorta converted to a smooth parametric surface.

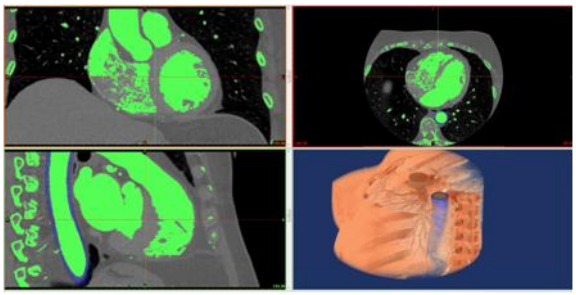

Medical Image (CT, MRI, Mimics)

Biomodeling of Aorta

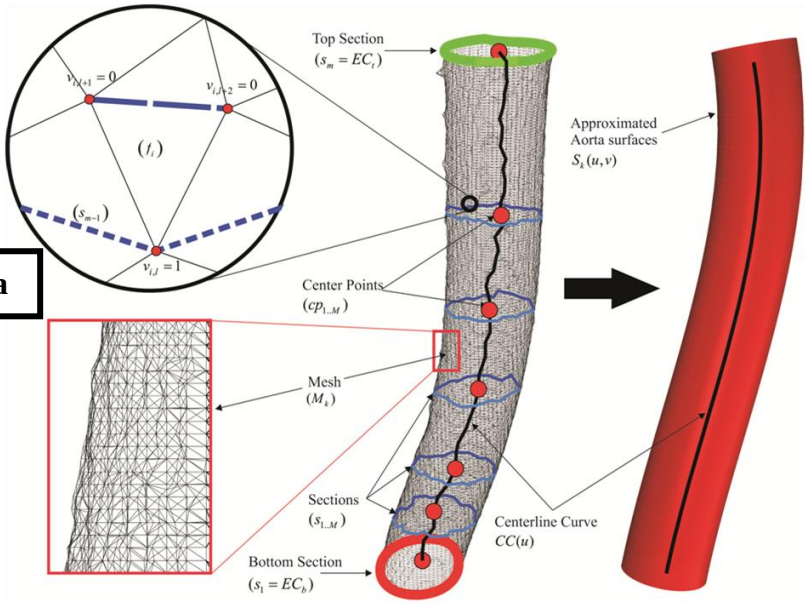

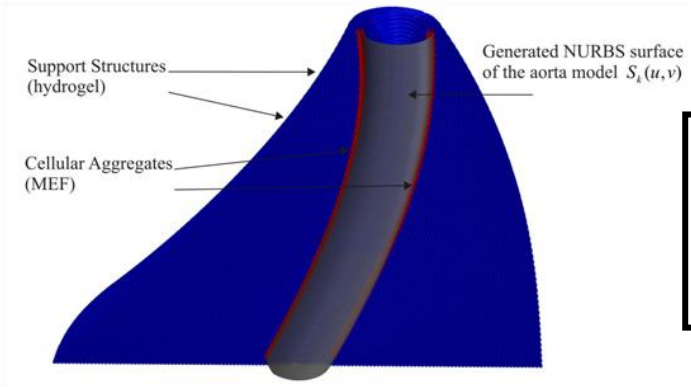

Optimization of Bioprinting Topology 'Self-Supporting' Model

3D Bioprinting

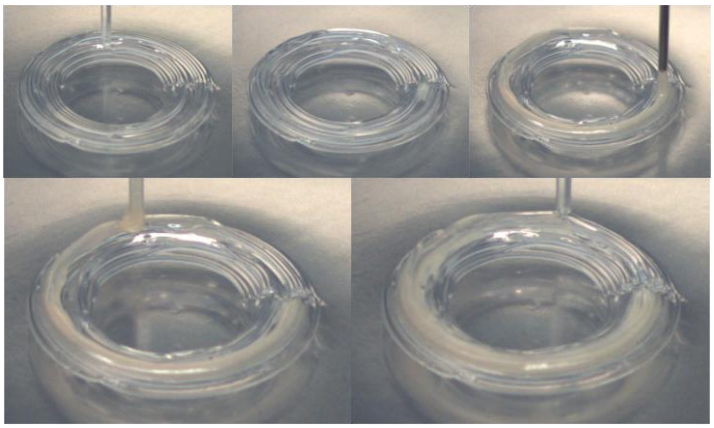

Figure 5.1. Roadmap of the proposed methodology

- The computer model is then sliced for the proposed layer-based 3D bioprinting process and the proposed methodology has been implemented in every slice to compute the locations for both cellular aggregates and support structures.

- To support the bioprinted live cell aggregates, a novel self-supporting methodology is developed. Self-supporting methodology is used to calculate corresponding locations for both cell aggregates and the support structures.

- The bioprinting topology is generated in order to mimic the aorta model from medical images, thus the cell aggregate and the support structure paths are generated. Both cellular aggregates (red cylinders) and hydrogels (blue cylinders) are necessarily placed on the valleys of the preceding layer to supply sufficient fusion conditions for the cellular aggregates (Figure 5.2).In order to prevent cell outflow and to preserve anatomically correct form of the aorta model, the support structures are printed first at a layer, and then the cellular aggregates are placed into the valleys that support structures created.

- The generated cell and support paths are used to control the Novogen MMX 3D Bioprinter for 3D printing of a biomimetic aortic construct. To increase the cell viability, a small amount of appropriate medium is preferably dropped on printed cell aggregates during printing process.

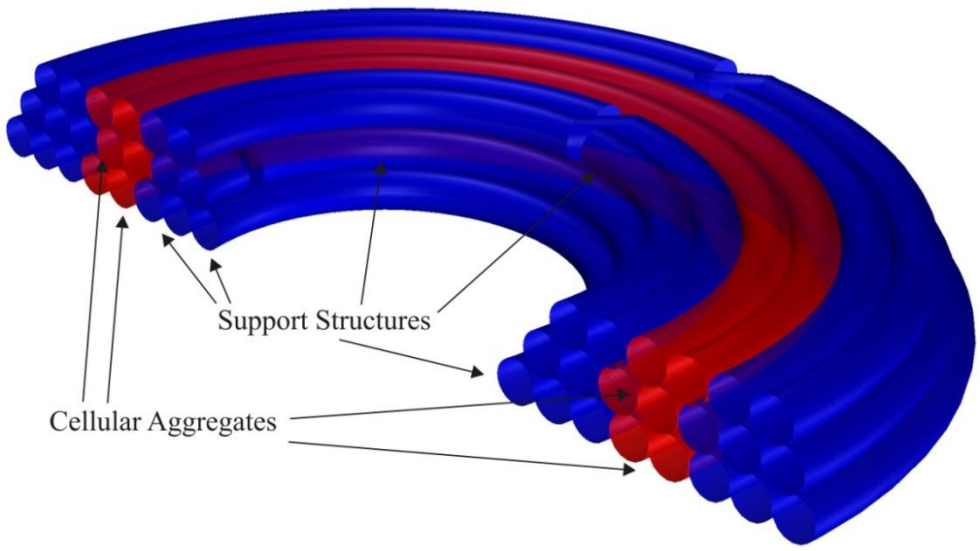

Figure 5.2. Three consecutive example layers showing how support structures (blue) and cellular aggregates (red) are placedon the valleys of the preceding layer.

5.3. Implementation and Results

The final outputs of the developed algorithms are 3D bioprinter instructions controlling the cell aggregate and support structure heads to build the tissue constructs layer by layer directly from the generated computer model.

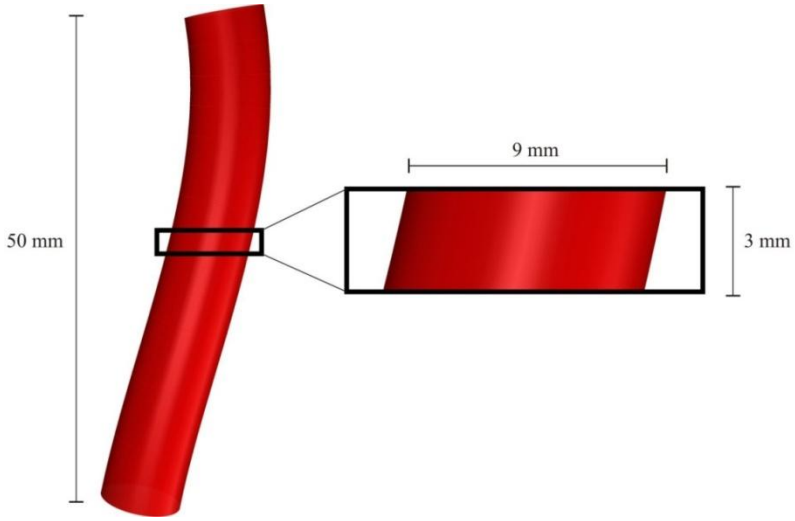

Figure 5.3. 3 mm (8 layer) part of aorta is extracted.

Because of the 3D printer capillary size, the original MR data is scaled down by almost 50%. The whole aorta surface model, which is extracted from the STL file, is 50 mm high and its diameter is around 9 mm. In this step, the extracted aorta's dimensions were exactly mimicked in bioprinting of both cellular aggregates and support structures. A partial aorta model with 3 mm height is extracted as shown in Figure 5.3 and its path planning for 3D bioprinting is obtained by developed algorithms. As illustrated in Figure 5.4, by the cross sectional view, blue cylinders are representing support structures, where red ones represent cell aggregates. The cell aggregates are covered with support layers which allow appropriate medium diffusion to provide increased cell viability.

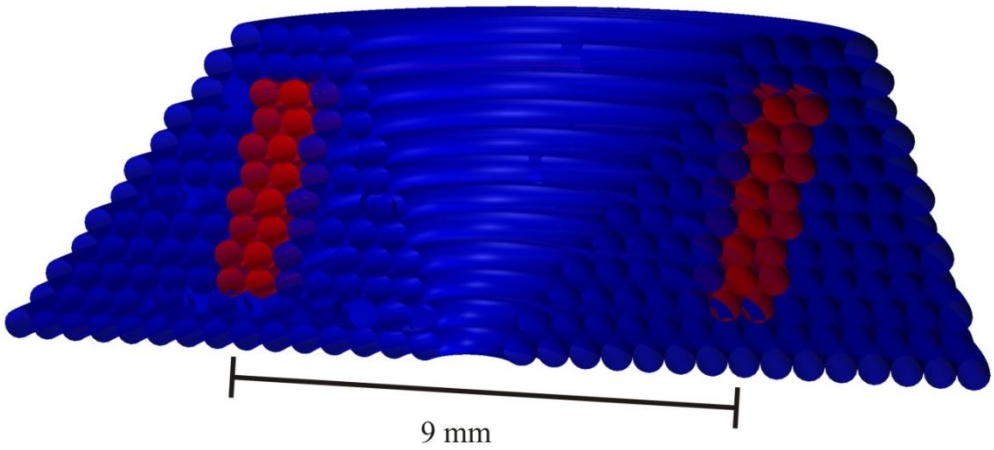

Figure 5.4. The cross sectional view of the aorta with support structures (blue) generated with respect to the Self-Supporting model and cellular aggregates (red)

The proposed method is tested with plain and red-colored hydrogels (red represents the cellular aggregates) as shown in Figure 5.5.

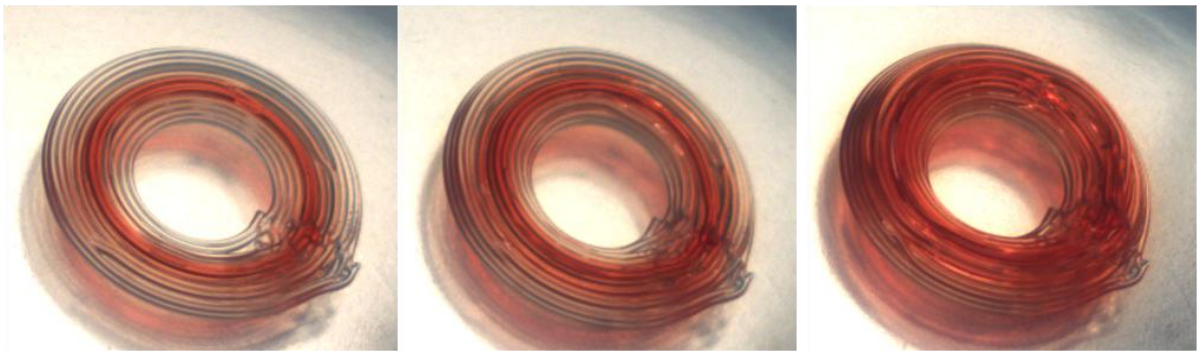

Figure 5.5. 3D printed hydrogels with ‘Self-Supporting’ model.

The modeled part of human aortic blood vessel was successfully 3D bioprinted in accordance with the developed algorithms [36, 49]. Different printing steps and printed structure in formaldehyde are shown in Figure 5.6.

The developed methods are used for bio-printing of mouse embryonic fibroblast (MEF) cells and human dermal fibroblast (HDF) cells, respectively. Cells are aggregated into cylinders of specific diameter (450 μm). MEF cell aggregates and support structures are 3D printed layer-by-layer according to the developed Self-Supporting method as shown in Figure 5.7 and in Figure 5.8.

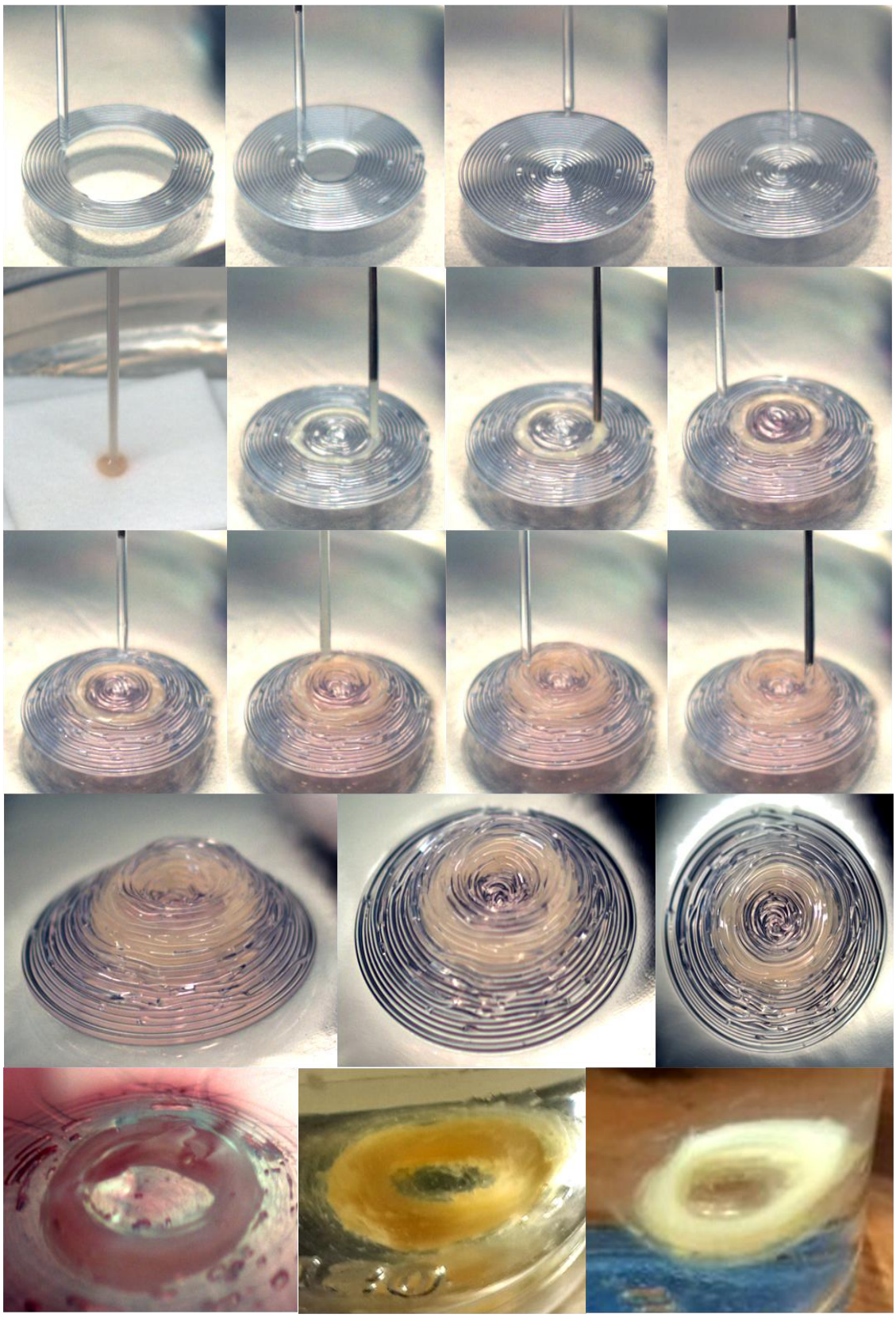

Figure 5.6. Different printing steps

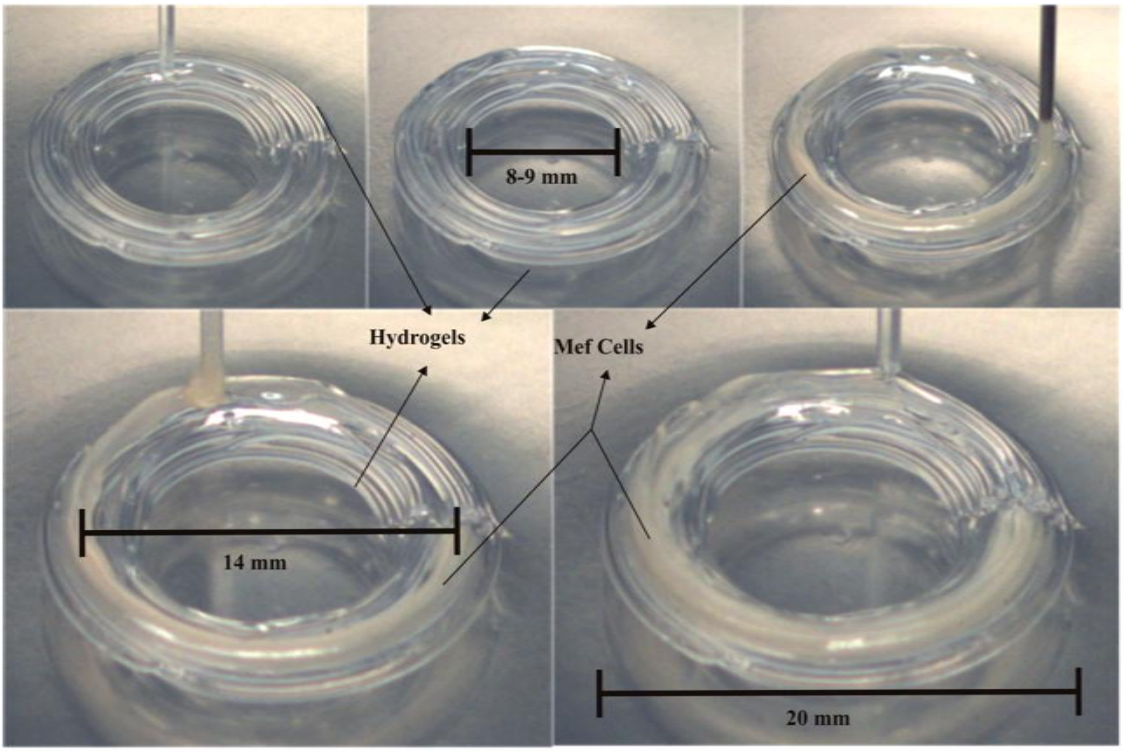

Figure 5.7. 3D printed MEF cell aggregates of originally mimicked aorta in 'Self-Supporting' model.

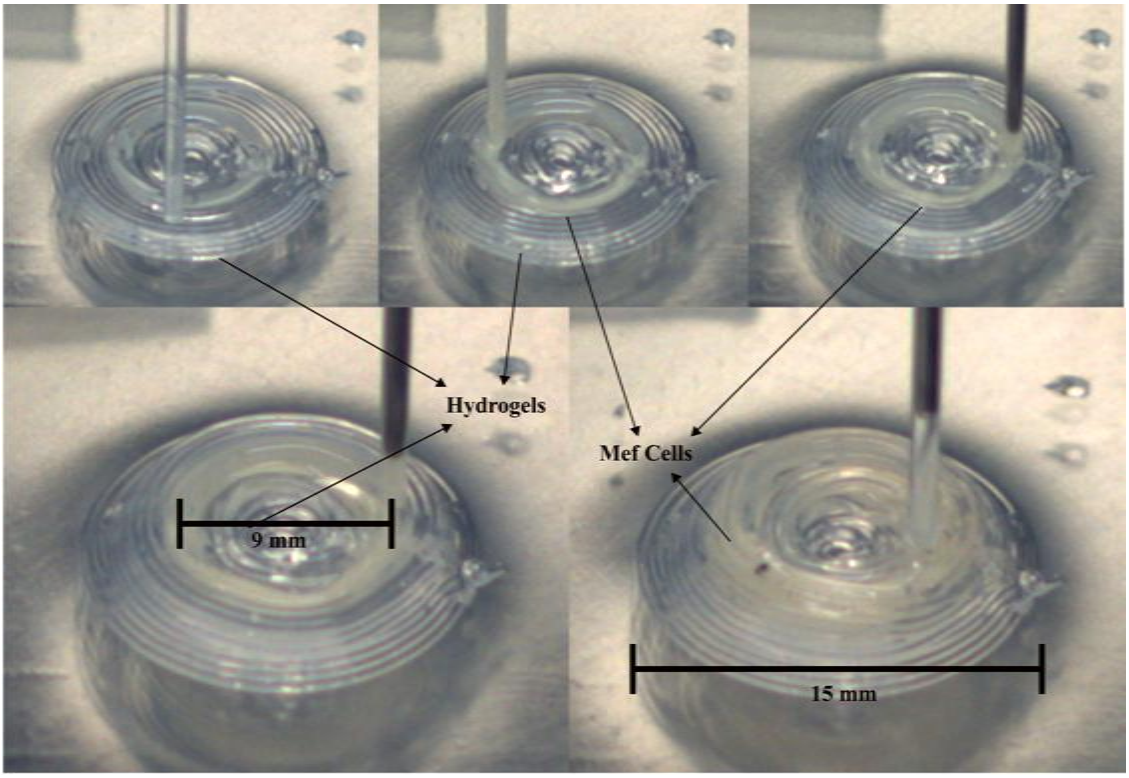

Figure 5.8. 3D printed MEF cell aggregates of 'Self-Supporting' model.

HDF cell aggregates and hydrogel support structures are also 3D bioprinted successfully according to the Self-Supporting model (Figure 5.9). The HDF cell aggregates are printed into the channels formed by the hydrogel support structure.

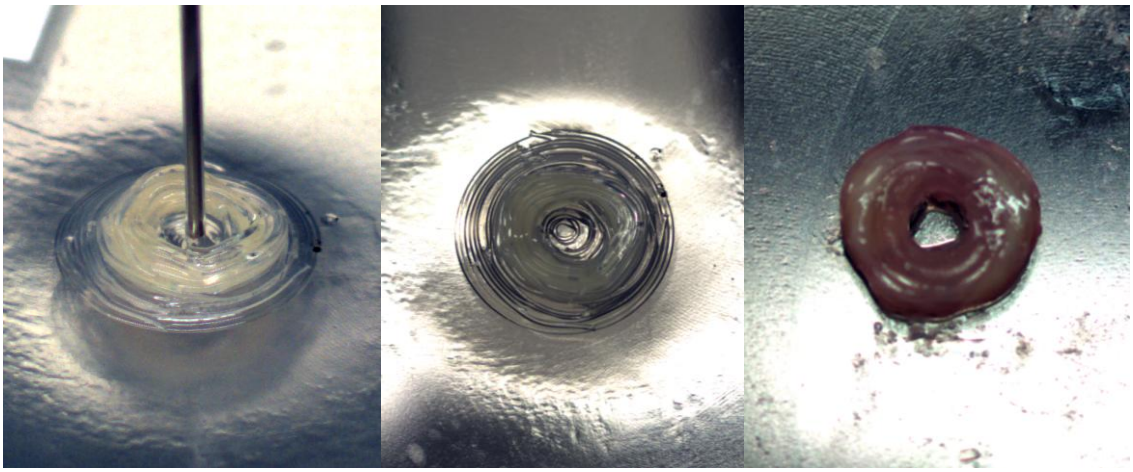

Figure 5.9. 3D bioprinted HDF cell aggregates with hydrogel support structure.

5.4. Discussion and Conclusion

In this chapter, novel methods are developed for 3D hybrid cell and biomaterial printing of macravascular structures directly from computer models. After imaging of a real human aorta, the captured geometry was converted to a mesh model. In order to develop path planning and topology optimization for 3D bioprinting, parametric surfaces are generated from the generated mesh model. A Self-Supporting model is developed in order to 3D bioprint MEF / HDF cell aggregates and hydrogel support structures layer by layer using the Novogen MMX 3D Bioprinter. Thus, a self-supporting scaffold-free artificial biological structure is constructed in bottom-up direction which biomimics a real human aorta. In literature, vascular grafts are fabricated by using cylindrical building blocks composed of hydrogel and matured cellular aggregates with a constant cross section [23, 24]. In some other studies, cell sheet based technology is used to create tubular blood vessels which do not biomimic a real human vessel [8, 27,30].The proposed method has a high reproducibility and does not require any manual intervention.

Thermo-reversible, bioinert NovoGel is used for printing the support structures. In future, other biomaterials may be considered in the production and design of

macrovascular structures. Additionally, a real blood vessel contains three different cell types including endothelial cells, smooth muscle cells and fibroblasts[24]. Therefore, this study may be extended to multicellular macrovascular structure by using endothelial, smooth muscle and fibroblast cells together.

CHAPTER 6

6. CONCLUSION and FUTURE DIRECTIONS

Bioprinting is one of the most promising techniques in tissue engineering, which is defined as depositing living cells layer-by-layer with or without biomaterials in user-defined patterns to build 3D tissue constructs. In 3D bioprinting, cell aggregates (bioink) are used as building blocks that are placed by the bioprinter into precise architecture according to developed computational algorithms. The maturation of the printed tissue construct occurs in an architecture that resembles the normal tissue or organ.

The NovoGen MMM^{TM} 3D bioprinter is used throughout this research work, which relies on fusion of multicellular aggregates. In previous studies, cylindrical multicellular aggregates preparation includes several steps where manual intervention was inevitable. Our proposed approach allows the automatic aspiration of cell aggregates into the capillary to form cylindrical cell aggregates. Cell aggregates in the capillary are compressed to assure that no gaps appear before printing and no droplet formation occurs due the surface tension. The relationship between the surface tension, viscosity of cell suspension and the compression ratio is calculated for a successful extrusion. The compression ratio is found to be 0.23. It should be considered that the rheological values of cell suspension, which are necessary for calculations, are taken from literature and they do not directly correspond with the cell types used in the implementations. However, this result is encouraging to extend the mathematical analyze after obtaining the matching rheological properties.

In this research, methodologies for totally automated 3D bioprinting of anatomically-correct tissue constructs are presented. However, there are some limitations with semi-continuous printing because the 3D bioprinter system is configured for capillary

deposition. Since the 3D bioprinter is equipped with 75/85 mm long capillaries, the maximum length of support structure or cell aggregates that can be extruded each time is limited. Therefore, the capillary is loaded with support structure or cell aggregates each time during the printing process which definitely slows down the process and prevents a full-continuous printing. The proposed bioprinting strategies enable the use of the maximum capillary volume for each extrusion and therefore provide a semi-continuous bioprinting process. As a future work, a bioprinter could be developed for uninterrupted printing of whole construct.

Live mouse embryonic fibroblast (MEF), human dermal fibroblast cells (HDF) aggregates and support materials (hydrogels) are 3D bioprinted layer-by-layer according to the developed computer models to form biomimetic aortic vessel structures. In future, the structure should be bioprinted using endothelial, smooth muscle and fibroblast cells together, and then perfused in an appropriate bioreactor for self-assembly and maturation to achieve mechanical properties necessary for implantation.

Based on the developed bioprinting strategies, multicellular aggregates and their support structures are bioprinted to form 3D tissue constructs with different shapes. The stripe shaped constructs composed of HUVEC/HDF cell aggregates were strong enough to be handled and transferred in comparison to the constructs composed of MOVAS/HUVEC/NIH 3T3 multicellular aggregates. Therefore, we plan to modify the experiments by using human aortic smooth muscle, endothelial and fibroblast cells. On the other hand, the deformation percentages of the printed constructs should be considered during the development of bioprinting strategies. Most importantly, the printed constructs show rapid fusion and high cell viability (97%) after printing. However, the current 3D bioprinting system has limitations to create large structures. Even the cells can survive the extrusion process; a large cell construct in an open environment may not survive a slow and therefore long printing process. Therefore, the 3D bioprinting system should be configured for continuous deposition using syringes with larger volumes.

Although the current 3D bioprinting technology shows a great deal of promise to generate 3D layered constructs using live mixed cell populations, there is still a long way to go to create a fully-functional organ.

BIBLIOGRAPHY

1. Langer R, Vacanti JP. Tissue engineering. Science. 1993;260(0036-8075 (Print)):920-6.

2. Pollok JM, Vacanti JP. Tissue engineering. Semin Pediatr Surg. 1996(1055-8586 (Print)):191-6.

3. Nakayama K. In Vitro Biofabrication of Tissues and Organs. In: Forgacs G, Sun W, editors. Biofabrication: Micro- and Nano-fabrication, Printing, Patterning and Assemblies: Elsevier; 2013. p. 1-16.

4. Wüst S, Müller R, Hofmann S. Controlled Positioning of Cells in Biomaterials—Approaches Towards 3D Tissue Printing. Journal of Functional Biomaterials. 2011;2(3):119-54.

5. Melchels FPW, Domingos MAN, Klein TJ, Malda J, Bartolo PJ, Hutmacher DW. Additive manufacturing of tissues and organs. Progress in Polymer Science. 2012;37(8):1079-104.

6. Khoda AKM, Ozbolat IT, Koc B. A functionally gradient variational porosity architecture for hollowed scaffolds fabrication. Biofabrication. 2011;3(3):034106.

7. Khoda AKM, Ozbolat IT, Koc B. Designing heterogeneous porous tissue scaffolds for additive manufacturing processes. Computer-Aided Design. 2013;45(12):1507-23.

8. Matsuda N, Shimizu T, Yamato M, Okano T. Tissue Engineering Based on Cell Sheet Technology. Advanced Materials. 2007;19(20):3089-99.

9. Koç B, Hafezi F, Ozler SB, Kucukgul C. Bioprinting-Application of Additive Manufacturing in Medicine. In: Bandyopadhyay A, Bose S, editors. Additive Manufacturing: CRC Press; in press.

10. Xu C, Chai W, Huang Y, Markwald RR. Scaffold-free inkjet printing of three-dimensional zigzag cellular tubes. Biotechnology and Bioengineering. 2012;109(12):3152-60.

11. Nahmias Y, Schwartz RE, Verfaillie CM, Odde DJ. Laser-guided direct writing for three-dimensional tissue engineering. Biotechnology and Bioengineering. 2005;92(2):129-36.

12. Zhang Y, Yu Y, Chen H, Ozbolat IT. Characterization of printable cellular micro-fluidic channels for tissue engineering. Biofabrication. 2013;5(2):025004.

13. Khatiwala C, Law R, Shepherd B, Dorfman S, Csete M. 3D cell bioprinting for regenerative medicine research and therapies. Gene Ther Regul. 2012;07(01):1230004.

14. Mironov V, Prestwich G, Forgacs G. Bioprinting living structures. Journal of Materials Chemistry. 2007;17(20):2054-60.

15. Organ, Doku Nakli ve Diyaliz Hüzmetleri Daire Baskanligi. Available from: https://organ.saglik.gov.tr/web/Default.aspx.

16. Nemeno-Guanzon JG, Lee S, Berg JR, Jo YH, Yeo JE, Nam BM, et al. Trends in tissue engineering for blood vessels. J Biomed Biotechnol. 2012;2012:14.

17. Germain L, Rémy-Zolghadri M, Auger F. Tissue engineering of the vascular system: From capillaries to larger blood vessels. Medical and Biological Engineering and Computing. 2000;38(2):232-40.

18. Hockaday LA, Kang KH, Colangelo NW, Cheung PYC, Duan B, Malone E, et al. Rapid 3D printing of anatomically accurate and mechanically heterogeneous aortic valve hydrogel scaffolds. Biofabrication. 2012;4(3):035005.

19. Duan B, Hockaday LA, Kang KH, Butcher JT. 3D Bioprinting of heterogeneous aortic valve conduits with alginate/gelatin hydrogels. Journal of Biomedical Materials Research Part A. 2012;101A(5):1255-64.

20. Daniela FDC, Andreas B, Michael W, Jörg J, Sabine N, Wilhelm J-D, et al. Three-dimensional printing of stem cell-laden hydrogels submerged in a hydrophobic high-density fluid. Biofabrication. 2013;5(1):015003.

21. Du Y, Ghodousi M, Qi H, Haas N, Xiao W, Khademhosseini A. Sequential assembly of cell-laden hydrogel constructs to engineer vascular-like microchannels. Biotechnology and Bioengineering. 2011;108(7):1693-703.

22. Bertassoni LE, Cecconi M, Manoharan V, Nikkhah M, Hjortnaes J, Cristino AL, et al. Hydrogel bioprinted microchannel networks for vascularization of tissue engineering constructs. Lab on a Chip. 2014;14(13):2202-11.

23. Norotte C, Marga FS, Niklason LE, Forgacs G. Scaffold-free vascular tissue engineering using bioprinting. Biomaterials. 2009;30(30):5910-7.

24. Marga F, Jakab K, Khatiwala C, Shepherd B, Dorfman S, Hubbard B, et al. Toward engineering functional organ modules by additive manufacturing. Biofabrication. 2012;4(2):022001.

25. Jakab K, Norotte C, Marga F, Murphy K, Vunjak-Novakovic G, Gabor F. Tissue engineering by self-assembly and bio-printing of living cells. Biofabrication. 2010;2(2):022001.

26. Faulkner-Jones A, Greenhough S, King JA, Gardner J, Courtney A, Shu W. Development of a valve-based cell printer for the formation of human embryonic stem cell spheroid aggregates. Biofabrication. 2013;5(1):015013.

27. L'Heureux N, Dusserre N, Konig G, Victor B, Keire P, Wight TN, et al. Human tissue-engineered blood vessels for adult arterial revascularization. Nat Med. 2006;12(3):361-5.

28. Yuji Haraguchi, Tatsuya Shimizu, Masayuki Yamato, Okano T. Regenerative Therapies Using Cell Sheet-Based Tissue Engineering for Cardiac Disease. Cardiology Research and Practice. 2011;2011.

29. Zhao J, Liu L, Wei J, Ma D, Geng W, Yan X, et al. A Novel Strategy to Engineer Small-Diameter Vascular Grafts From Marrow-Derived Mesenchymal Stem Cells. Artif Organs. 2012;36(1):93-101.

30. L'Heureux N, Pâquet S, Labbé R, Germain L, Auger FA. A completely biological tissue-engineered human blood vessel. The FASEB Journal. 1998;12(1):47-56.

31. Gwyther TA, Hu JZ, Christakis AG, Skorinko JK, Shaw SM, Billiar KL, et al. Engineered Vascular Tissue Fabricated from Aggregated Smooth Muscle Cells. Cells Tissues Organs. 2011;194(1):13-24.

32. Gwyther TA, Hu Jz Fau - Billiar KL, Billiar Kl Fau - Rolle MW, Rolle MW. Directed cellular self-assembly to fabricate cell-derived tissue rings for biomechanical analysis and tissue engineering. Journal of Visualized Experiments. 2011(1940-087X (Electronic)).

33. Adebayo O, Hookway TA, Hu JZ, Billiar KL, Rolle MW. Self-assembled smooth muscle cell tissue rings exhibit greater tensile strength than cell-seeded fibrin or collagen gel rings. Journal of Biomedical Materials Research Part A. 2013;101A(2):428-37.

34. Christopher MO, Francoise M, Gabor F, Cheryl MH. Biofabrication and testing of a fully cellular nerve graft. Biofabrication. 2013;5(4):045007.

35. Mironov V, Kasyanov V, Markwald RR. Organ printing: from bioprinter to organ biofabrication line. Curr Opin Biotechnol. 2011;22(5):667-73.

36. Kucukgul C, Ozler B, Karakas HE, Gozuacik D, Koc B. 3D Hybrid Bioprinting of Macrovascular Structures. Procedia Engineering. 2013;59(0):183-92.

37. ImageJ, Image Processing and Analysis in Java [15.07.2014]. Available from: http://imagej.nih.gov/ij/.

38. Brian C, Gary N, Sunghwan J. Drop formation from a wettable nozzle. Commun Nonlinear Sci Numer Simul. 2012;17(5):2045-51.

39. Forgacs G, Kosztin I. Cellular aggregates under pressure. American Physical Society. 2010;3.

40. Iordan A, Duperray A Fau - Verdier C, Verdier C. Fractal approach to the rheology of concentrated cell suspensions. Phys Rev E Stat Nonlin Soft Matter Phys. 2008(1539-3755 (Print)).

41. Norotte C, Marga F, Neagu A, Kosztin I, Forgacs G. Experimental evaluation of apparent tissue surface tension based on the exact solution of the Laplace equation. EPL (Europhysics Letters). 2008;81(4):46003.

42. Preziosi L, Ambrosi D, Verdier C. An elasto-visco-plastic model of cell aggregates. J Theor Biol. 2010;262(1):35-47.

43. Zhang W, Wang S, Lin M, Han Y, Zhao G, Jian Lu T, et al. Advances in experimental approaches for investigating cell aggregate mechanics. Acta Mechanica Solida Sinica. 2012;25(5):473-82.

44. Lautrup B. Surface Tension. Physics of Continuous Matter, Exotic and everyday Phenomena in the Macroscopic World Second Edition ed2009. p. 69-94.

45. B. GD. Shear rheology of hard-sphere, dispersed, and aggregated suspensions, and filler-matrix composites. Advances in Colloid and Interface Science. 2012.

46. Roberts MT, Mohraz A Fau - Christensen KT, Christensen Kt Fau - Lewis JA, Lewis JA. Direct flow visualization of colloidal gels in microfluidic channels. Langmuir. 2007;23(0743-7463 (Print)):8726-31.

47. Bird RB, Warren SE, Lightfoot EN. Transport Phenomena. Second ed: Wiley; 2002.

48. Aguado BA, Mulyasasmita W Fau - Su J, Su J Fau - Lampe KJ, Lampe Kj Fau - Heilshorn SC, Heilshorn SC. Improving viability of stem cells during syringe needle flow through the design of hydrogel cell carriers. Tissue Engineering: Part A. 2012;18(1937-335X (Electronic)):806-15.

49. Kucukgul Can, Ozler Saime Burce, Inci İlyas, Irmak Ster, Gozuacik Devrim, Taralp Alpay, et al. 3D Bioprinting of Biomimetic Aortic Vascular Constructs with Self-Supporting Cells. Bioengineering and Biotechnology. submitted in 2014.

50. Mimics, Medical Image Segmentation for Engineering on Anatomy [10.11.2013]. Available from: http://biomedical.materialise.com/mimics.